NPS-62-88-006

NAVAL POSTGRADUATE SCHOOL
Monterey, California

THESIS

NUMERICAL ELECTROMAGNETIC MODELS OF CUBE-SHAPED BOXES--AN INITIAL INVESTIGATION FOR NEAR-FIELD PREDICTION OF HF SHIPBOARD ENVIRONMENTS

by

Carlos R Molina T

December 1987

Thesis Advisor: R. W. Adler

Prepared for:
Naval Ocean Systems Center
San Diego, CA 92152

NAVAL POSTGRADUATE SCHOOL
Monterey, California 93943-5000

Rear Admiral R.C. Austin
Superintendent

K.T. Marshall
Acting Provost

This thesis is prepared in conjunction with research sponsored in part by Naval Ocean Systems Center under N6227186WR60125.

Reproduction of all or part of this report is authorized.

Released by:

Gordon E. Schacher
Dean of Science and Engineering

UNCLASSIFIED
SECURITY CLASSIFICATION OF THIS PAGE

REPORT DOCUMENTATION PAGE

1a. REPORT SECURITY CLASSIFICATION UNCLASSIFIED	1b. RESTRICTIVE MARKINGS
2a. SECURITY CLASSIFICATION AUTHORITY	3. DISTRIBUTION/AVAILABILITY OF REPORT Approved for public release; distribution is umlimited
2b. DECLASSIFICATION/DOWNGRADING SCHEDULE	
4. PERFORMING ORGANIZATION REPORT NUMBER(S) NPS-62-88-006	5. MONITORING ORGANIZATION REPORT NUMBER(S)
6a. NAME OF PERFORMING ORGANIZATION Naval Postgraduate School 6b. OFFICE SYMBOL (If applicable) 62	7a. NAME OF MONITORING ORGANIZATION Naval Postgraduate School
6c. ADDRESS (City, State, and ZIP Code) Monterey, California 93943-5000	7b. ADDRESS (City, State, and ZIP Code) Monterey, California 93943-5000
8a. NAME OF FUNDING/SPONSORING ORGANIZATION Naval Ocean Systems Center 8b. OFFICE SYMBOL (If applicable)	9. PROCUREMENT INSTRUMENT IDENTIFICATION NUMBER N6227186WR60125
8c. ADDRESS (City, State, and ZIP Code) San Diego, California 92152	10. SOURCE OF FUNDING NUMBERS PROGRAM ELEMENT NO. / PROJECT NO. / TASK NO / WORK UNIT ACCESSION NO

11. TITLE (Include Security Classification) NUMERICAL ELECTROMAGNETIC MODELS OF CUBE-SHAPED BOXES--AN INITIAL INVESTIGATION FOR NEAR-FIELD PREDICTION OF HF SHIPBOARD ENVIRONMENTS

12. PERSONAL AUTHOR(S)
Carlos R Molina T

13a. TYPE OF REPORT	13b TIME COVERED	14. DATE OF REPORT (Year, Month, Day)	15 PAGE COUNT
Master's Thesis	FROM _____ TO _____	1987 December	86

16. SUPPLEMENTARY NOTATION

17. COSATI CODES			18. SUBJECT TERMS (Continue on reverse if necessary and identify by block number)
FIELD	GROUP	SUB-GROUP	Near Fields Prediction; Numerical Electromagnetic; Code NEC

19. ABSTRACT (Continue on reverse if necessary and identify by block number)

An investigation was performed to evaluate the accuracy of numerical modeling of near fields for antennas on or near surfaces using the Numerical Electromagnetic Code (NEC). Average power gain and input impedance were calculated, for two models. The first, a dipole antenna located inside a cube-shaped wire-grid box of 1 meter sides was evaluated for a wide range of frequencies in free space. The second, a monopole antenna mounted on the top of two cube shaped boxes (a wire grid and surface patch box) of .1 meter sides over a perfectly conducting ground was evaluated from 1 to 1.4 GHz. The monopole was positioned at the center, at an edge, and at the corner of the box top. For the dipole in the box, the average gain and input impedance are presented and evaluated. For the monopole on the box, calculated results are compared to measured admittance values. The NEC wire-grid model results compare closely to the measurements, but for surface-patch models, only one,

20. DISTRIBUTION/AVAILABILITY OF ABSTRACT	21. ABSTRACT SECURITY CLASSIFICATION	
☒ UNCLASSIFIED/UNLIMITED ☐ SAME AS RPT ☐ DTIC USERS	UNCLASSIFIED	
22a. NAME OF RESPONSIBLE INDIVIDUAL R. W. Adler	22b. TELEPHONE (Include Area Code) (408) 646-2352	22c. OFFICE SYMBOL 62Ab

DD FORM 1473, 84 MAR 83 APR edition may be used until exhausted
All other editions are obsolete

SECURITY CLASSIFICATION OF THIS PAGE
UNCLASSIFIED

19. Abstract (continued)

position of the monopole yielded satisfactory correlation to measurements. Recommendations for improved numerical modeling performance are made. (Theses) E

Approved for public release; distribution is unlimited.

Numerical Electromagnetic Models of Cube-Shaped Boxes--An Initial Investigation for Near-Field Prediction of HF Shipboard Environments

by

Carlos R Molina T
Lieutenant Commander, Venezuelan Navy
B.S., Venezuelan Naval Academy, 1975

Submitted in partial fulfillment of the
requirements for the degree of

MASTER OF SCIENCE IN ELECTRICAL ENGINEERING

from the

NAVAL POSTGRADUATE SCHOOL
December 1987

Author: 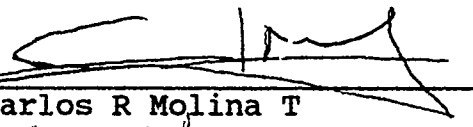
Carlos R Molina T

Approved by: 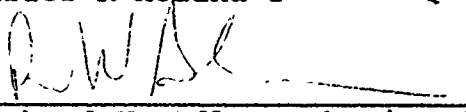
Richard W. Adler, Thesis Advisor

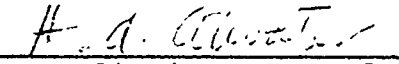
Harry Atwater, Second Reader

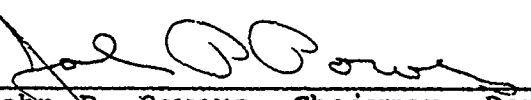
John P. Powers, Chairman, Department of
Electrical and Computer Engineering

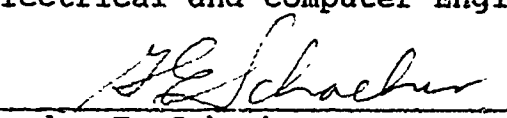
Gordon E. Schacher
Dean of Science and Engineering

ABSTRACT

An investigation was performed to evaluate the accuracy of numerical modeling of near-fields for antennas on or near surfaces using the Numerical Electromagnetic Code (NEC). Average power gain and input impedance were calculated, for two models. The first, a dipole antenna located inside a cube-shaped wire-grid box of 1 meter sides was evaluated for a wide range of frequencies in free space. The second, a monopole antenna mounted on the top of two cube shaped boxes (a wire grid and a surface patch box) of .1 meter sides over a perfectly conducting ground was evaluated from 1 to 1.4 GHz. The monopole was positioned at the center, at an edge, and at the corner of the box top. For the dipole in the box, the average gain and input impedance are presented and evaluated. For the monopole on the box, calculated results are compared to measured admittance values. The NEC wire-grid model results compare closely to the measurements, but for surface-patch models, only one position of the monopole yielded satisfactory correlation to measurements. Recommendations for improved numerical modeling performance are made.

TABLE OF CONTENTS

LIST OF TABLES

LIST OF FIGURES

ACKNOWLEDGEMENTS

I am indebted to those who have contributed their encouragement, assistance, and patience before and during the preparation of this thesis.

First, to Dr. Richard W. Adler, my thesis advisor, I want to express my thanks for his patient and unfailing guidance throughout this work.

To the Venezuelan Navy, I express my sincere appreciation for giving me the opportunity to earn my Master's degree.

Finally, I would like to thank my wife, Ana, my daughter, Anna, and my little boy Carlos for their support, understanding, and patient help through my time at the Naval Postgraduate School.

I. INTRODUCTION

A. GENERAL BACKGROUND

Because shipboard operations are carried out within fixed (small) distances from transmitting antennas, the Navy has a unique and long-standing operational problem: the radiation from these antennas can be dangerous to personnel, ordnance, fuel, and electronic equipment. This is called RADIATION HAZARD (RADHAZ).

Accordingly, the Navy has been pursuing the study of near fields of antennas for a number of years. However, the near field structure is complex, and previous theoretical analysis has been practical only for simple antennas in uncomplicated geometrical settings. With the advent of the modern high-speed computer, approximate solution techniques such as the method of moments used by the Numerical Electromagnetic Code have become practical.[Ref. 1]

B. NEED FOR STUDY

With the added emphasis on near field (due to RADHAZ) by EPA and USN demands, we must be more accurate in our near field predictions to assure that personnel and equipment can continue to function safely in modern shipboard RF environments.

C. SCOPE AND LIMITATIONS

Two theoretical models of cube shaped boxes (similar to those found on structures on shipboard systems) are examined. These boxes are modeled numerically and the parameters of one of the models is compared to measured values from Reference 2. Modeling techniques are varied to assess their impact on accuracy. Guidelines are developed for maximum accuracy. Also, it is known that the Numerical Electromagnetic Code has been found to suffer loss of accuracy in VLF applications involving electrically small antennas [Refs. 3 and 4]. This may affect the modeling efforts of this thesis.

II. NEAR FIELD THEORY

A. EXTERIOR FIELDS OF RADIATING ANTENNAS

Figure 2.1 describes the regions into which the exterior fields of a radiating antenna are commonly divided. The antenna radiates into free space as a linear system with the single-frequency time dependence of $e^{(-j\omega t)}$.

The **FAR-FIELD** region extends to infinity and is that region of space where the radial dependence of electric and magnetic fields varies approximately as $e^{(-jkr)}/r$. The inner radius of the far field can be estimated from the general free-space integral for the vector potential and is usually set at $\lambda + (2D^2/\lambda)$. (The added λ covers the possibility of the maximum dimension D of the antenna being smaller than a wavelength. In other words, the **RAYLEIGH** distance (Z)[1] should actually be measured from the outer boundary of the reactive near field of the antenna.) For the main beam direction, the **RAYLEIGH** distance can sometimes be reduced.

The free-space region from the surface of the antenna to the far field is labeled as the **NEAR-FIELD** region. It is divided into two subregions, the reactive and the

---

[1] The Rayleigh distance is given by $Z_d = \pi D^2/\lambda$

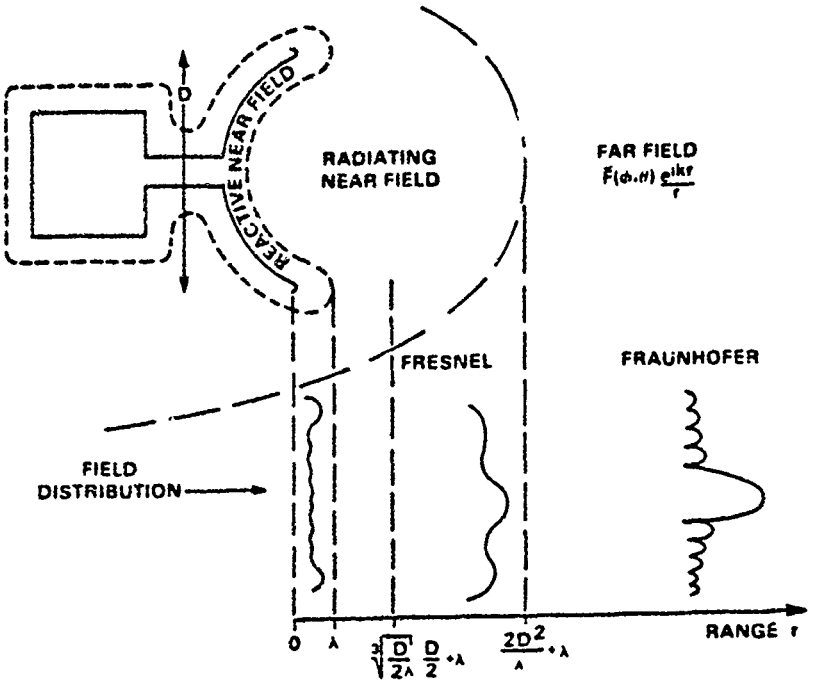

Figure 2.1 Exterior fields of radiating antennas [Ref.5].

radiating near fields. The reactive near-field region is commonly thought to extend about $\lambda/2\pi$ from the surface of the antenna, although experience with near-field measurements indicates that a distance of a wavelength (λ) or so would be a more reasonable outer boundary to the reactive near field.

The reactive near field can be defined in terms of planar, cylindrical, or spherical modes. Unfortunately, the reactive fields of spherical (or cylindrical) multipoles are not identical to the plane-wave evanescent fields of multipoles. Thus, a simpler, physically appealing and less ambiguous method of defining the reactive region of antennas

relies directly on Poynting's theorem and the vector potential. It can be shown that the contribution to the reactive part of the input impedance of an antenna from the fields outside a surface surrounding the antenna is proportional to the imaginary part of the complex Poynting vector integrated over the surface. Thus, wherever the phase of the electric and the magnetic field vectors are near quadrature, the Poynting vector will contribute mainly to the reactive part of the input impedance. Taking the curl of the vector potential integral once to get the magnetic field and twice to get the electric field, shows that the phase of the electric and magnetic fields may be near quadrature in regions within approximately a wavelength (λ) of the antenna. Consequently, the region within about a wavelength of the physical antenna is referred to as the **REACTIVE NEAR FIELD.**

Beyond a distance of about a wavelength, the electric and magnetic fields tend to propagate predominantly in phase, but, of course, do not exhibit $e^{(-jkr)}/r$ dependence until the far field is reached. This propagating region between the reactive near field and the far field is called the **RADIATING NEAR FIELD.**

Finally, the optical terms "Fraunhofer region" and "Fresnel region" are sometimes used to characterize the fields of antennas. The term **FRAUNHOFER REGION** can be used synonymously with the far-field region or to refer to the

focal region of an antenna focused at a finite distance. The **FRESNEL REGION**, which extends from about $(D/2\lambda)^{1/3}$ D/2 + λ to the far field, is the region up to the far field in which a quadratic phase approximation can be used in the vector potential integral. The Fresnel region is a sub-region of the radiating near-field region.[Ref. 5:pp. 33-34]

B. DIFFICULTIES WITH NEAR FIELD CALCULATIONS

The **NEAR FIELD** is more difficult to calculate than the far field. When calculating the near zone radiation, the antenna no longer appears as an infinitesimal point (as is the assumption for far field), but rather we are conscious that the energy coming toward us comes from separated locations. Also the terms of the field expressions with powers of 1/r (r is the distance from the origin of the antenna to the field point) greater than one are here more important than the 1/r-dependent terms. The complex **Poynting** vector $\frac{1}{2}(\vec{E} \times \vec{H}^*)$ will then contain terms with a power of (1/r) in addition to the radiation field term. It results that these terms are purely imaginary, indicating reactive power and energy oscillating in and out. The near field is restricted to charge and current density and far field only to current. All these difficulties make the near field calculation more imprecise.

In the past, accuracy of near-field calculations was not a problem; there was no practical application to which the energy could be applied. However, in recent years there has

been an escalating interest in the close-in problem, especially in the Navy where, in general, antennas mounted on a ship will couple into metallic parts of the ship. This means that strong RF currents can be excited on closely coupled conducting surfaces, which in turn re-radiate. The total near field is the (vector) sum of the fields radiated by the antenna, the primary antenna, and the nearby conducting objects. Re-radiation is enhanced whenever the secondary scatterers are similar in size to the prymary antennas or whenever resonant length conducting paths and spacing occur. Because of this the near field produces RADIATION HAZARD (RADHAZ) that can affect personnel, ordnance, and fuel on ships.

III. NUMERICAL MODELS OF SURFACE TYPE STRUCTURES

A. NUMERICAL MODELING OF SURFACES FOR NEAR-FIELD PREDICTION

There are two principal ways in which the method of moments can be used to model antennas together with the surrounding structures. The simplest way to model a solid surface is with a grid of wires, the so-called wire-grid model. The other approach is to divide the surface into patches or cells, each having a continuous metallic surface. This is the so-called surface-patch model.

The successful substitution of a wire grid or surface patch for a continuous metallic surface depends upon the fact that as the model (the wire grid or surface patch) becomes smaller relative to a wavelength, it supports a current distribution which approximates that of the continuous surface. The current is only an approximation to the actual current, however, and as such it can be expected to accurately predict the far fields but not necessarily the near fields. This is due to the fact that the wire-grid model supports an evanescent reactive field on both sides of its surface. An actual continuous conducting surface is not capable of supporting such a field. For surface patches the current is assumed to be continuous over a patch which is only a simple approximation to the current and allows no smooth variation over the body being modeled.

The version of the Numerical Electromagnetic Code that will be used in this work is **NEC-3**, although it has been reported by Burke [Refs. 3 and 4] that there are some inaccuracies in **NEC**. In the first model, the wire grid with interior dipole, there are some frequencies in which the wavelengths, are more than ten-times larger than the side dimension of the cell segments, and this may affect results. To increase confidence in the accuracy of the results, two antenna parameters are calculated: the average power gain and the input impedance. The average power gain provides a good check of the solution accuracy if it is close to one for free space or close to two for a perfectly conducting ground plane. For our purposes we will consider average power gain within ±10% of theoretical to be adequate for engineering purpose. Correct average power gain does not insure accurate near-field prediction. Therefore, input impedance, which is in general complex, is also checked. The real part of the impedance relates to radiated far-field power while the imaginary portion relates to the balance of reactive energy in the near field.

In the first model analyzed, the wire grid with a dipole inside, there are no measured values for comparison. In the second model, the wire-grid box with the monopole, the measured admittance is available. The next section describes these two models.

B. WIRE GRID BOX WITH INTERIOR DIPOLE

A WIRE-GRID box with an interior dipole was modeled to obtain numerical values of average power gain and input impedance. The model constructed was a 2 meter per side cube-shaped box, with a dipole inside, 1 Meter long. The grid was .4 by .4 meter cells, with each cell side divided into two segments (see Figure 3.1). (Initial wire grid box models employed both one and two segments per cell side and favored 2 segments per side as opposed to the conventional 1 segment per side.) The model was run at selected frequencies from 3 to 450 MHz, in free space. These parameters were chosen to span geometry parameters where guidelines for NEC wire modeling have been presented. These guidelines were:

1. Ratio between segment length (D) and segment radius (a) greater than or equal to two.
2. Angle between wires greater than $2\pi(D/a)^{-1}$
3. Spacing between segments greater than or equal to 10a.

Theoretically, this wire-grid box with the dipole inside should radiate. Therefore, average power gain and input impedance will be calculated. If acceptable values are obtained, a statement concerning the accuracy of near-field calculations via NEC can be prepared. In this case, average power gain must be close to one (free space). Values of acceptable input impedance must be limited to those where the ratio of the real to the imaginary part are less than 10^4. This limit is because of the accuracy of calculating complex numbers in NEC.

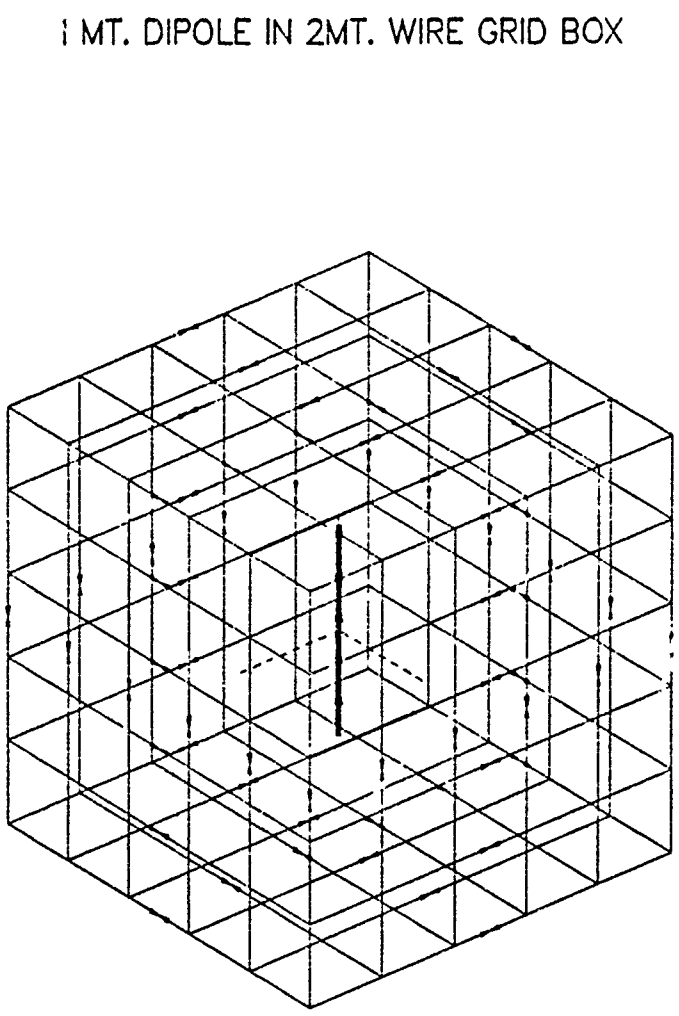

Figure 3.1 1 Meter Dipole in 2 Meter Wire-Grid Box.

C. MONOPOLE ON WIRE GRID BOX

Bhattacharya, Long and Wilton [Ref. 2] performed an experimental investigation to determine the input admittance characteristics of a monopole antenna mounted on a conducting cubical box over a ground plane. In this case, a 6 cm. monopole was positioned at the center, edge, and corner on the top of the box and the admittance was measured (see Table 1). This measured data [Ref. 2] was compared with calculated data obtained using a five-sided WIRE-GRID BOX model of .1 meter per side and cells of .0125 by .0125 meters.

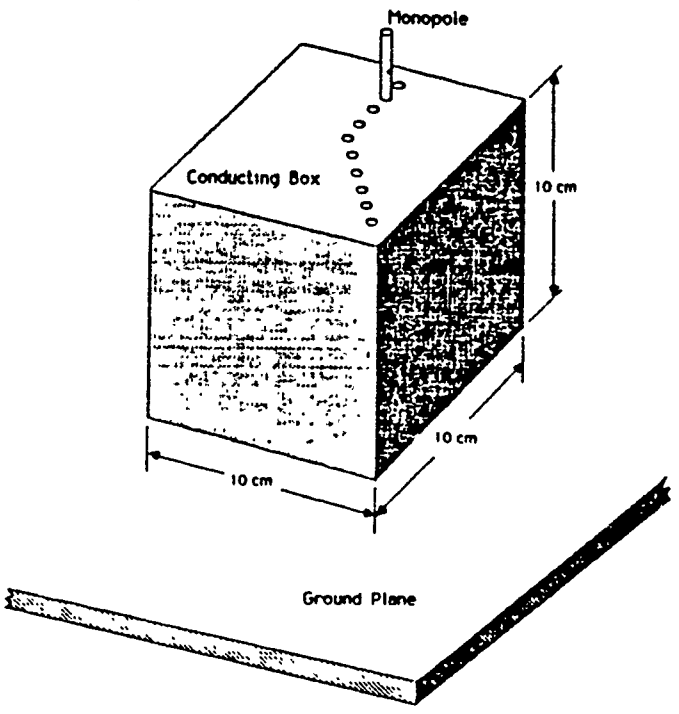

Figure 3.2 Geometry of a Monopole Mounted on a Cube Shaped Box Over a Ground Plane. [From Ref. 2]

TABLE 1

MEASURED DATA FOR A 6 CM. MONOPOLE ON A CUBE BOX [REF.2]

FREQUENCY GHZ.	6 cm. MONOPOLE POSITION		
	AT CENTER	AT EDGE 3.50cm FROM CENTER	AT CORNER 5.15cm. FORM CENTER
	ADMITTANCE		
1.0 GHZ.	5.00+j20.0	7.00+j17.0	7.00+j14.0
1.05 GHZ.	14.0+j28.0	1.05+j20.0	12.0+j13.0
1.1 GHZ.	37.0+j18.0	24.0+j17.0	18.0+j10.0
1.15 GHZ.	41.0-j8.00	32.0+j2.00	21.0+j4.00
1.2 GHZ.	26.0-j16.0	26.0-j7.00	20.0-j2.00
1.225GHZ.	19.0-j15.0	26.0-j11.0	17.0-j4.50
1.3 GHZ.	11.0-j10.0	12.0-j9.00	12.0-j5.00
1.4 GHZ.	7.00-j6.00	7.00-j5.00	8.00-j3.00

In order to simulate the cube box in Figure 3.2, a model of a 6 cm. monopole divided into 5 segments was placed on top of the wire-grid box at the center (see Figure 3.3), at the edge 3.75 cm. from the center (see Figure 3.4), and at the corner 5.3 cm. from the center (see Figure 3.5). The feed of the antenna was placed at the base and second segment up on the monopole at the center of the wire grid only to see if there was any major difference in the results.

The calculated average power gain and input impedance are shown in Tables 2, 3, and 4.

D. MONOPOLE ON SURFACE PATCH BOX

In the same fashion as the wire grid box, a five sided SURFACE-PATCH BOX of .1 meter per side and cells .02 by .02 meters was constructed in order to simulate the cubical box described in Reference 1. For this model, two different tops of the cube were designed to allow placement of the model of a 6 cm. monopole divided into five segments at the center (see Figure 3.6), at the edge 3.5 cm. from the center (see Figure 3.7) and at the corner 4.93 cm. from center (see Figure 3.8). In each case, the monopole was fed at the base segment.

The calculated average power gain and input impedance are shown in Tables 5, 6, and 7, and description of the results are discuss in Chapter V.

6 CM. MONOPOLE AT CENTER OF WIRE GRID BOX

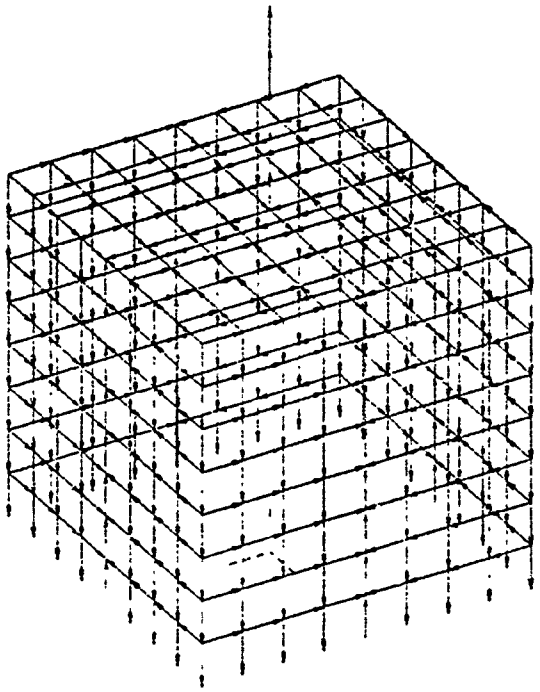

THETA = 60.00 PHI = 60.00 ETA = 90.00

Figure 3.3 6 cm. Monopole at Center of Wire-Grid Box.

6 CM. MONOPOLE AT EDGE 3.75 CM. FROM CENTER

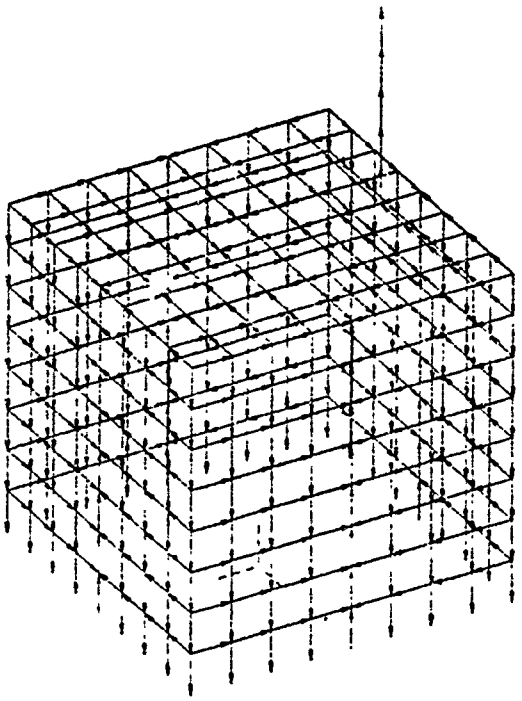

THETA = 60.00 PHI = 60.00 ETA = 90.00

Figure 3.4 6 cm. Monopole at Edge 3.75 cm. from Center.

6 CM. MONOPOLE AT CORNER 5.3 CM. FROM CENTER

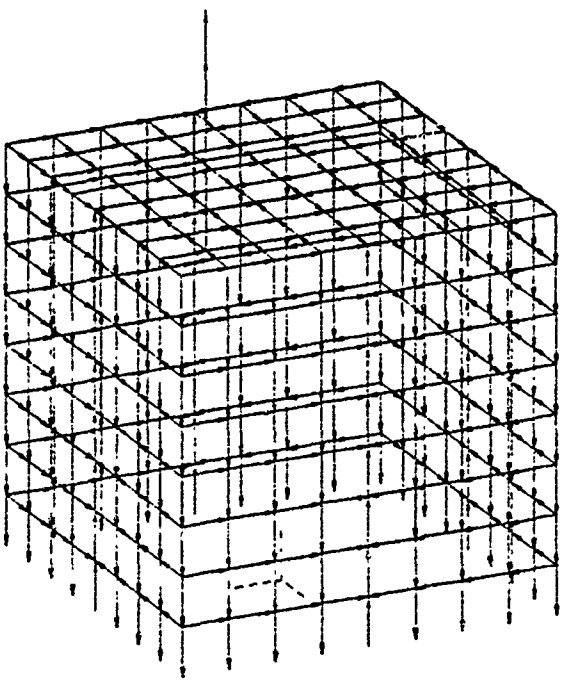

THETA = 70.00 PHI = 65.00 ETA = 90.00

Figure 3.5 6 cm. Monopole at Corner 5.3 cm. from Center.

TABLE 2

CALCULATED DATA FOR A MONOPOLE AT THE CENTER
OF A WIRE-GRID BOX, BASE SEGMENT FEED

FREQUENCY GHZ.	AVG. Power Gain		IMPEDANCE / ADMITTANCE		
	1 Seg.	2 Seg.	1 Seg.	2 Seg.	AVG. 1-2Seg.
1.0 GHZ.	1.76	1.87	13.0-j40.7 7.15+j22.2	15.1-j45.4 6.49+j19.6	14.1-j43.0 6.82+j20.9
1.05 GHZ.	1.79	1.91	16.8-j23.3 20.3+j28.2	17.9-j25.5 18.4+j26.3	17.4-j24.4 19.4+j27.3
1.1 GHZ.	1.8	1.93	21.6-j6.60 42.4+j13.0	24.1-j7.00 38.2+j11.1	22.9-j6.80 40.3+j12.0
1.15 GHZ.	1.82	1.94	27.4+j9.30 32.7-j11.1	29.2+j10.3 30.4-j10.7	28.3+j9.80 31.6-j10.9
1.2 GHZ.	1.83	1.96	34.3+j24.1 19.5-j13.7	36.9+j27.4 17.4-j13.0	35.6+j25.8 18.5-j13.4
1.3 GHZ.	1.84	1.97	50.3+j50.0 10.0-j10.8	52.1+j56.2 8.88-j9.57	51.2+j53.1 9.44-j10.2
1.4 GHZ.	1.86	1.98	66.7+j70.6 7.07-j7.48	66.8+j79.0 6.24-j7.38	66.8+j74.8 6.70-j7.43

TABLE 3

CALCULATED DATA FOR A MONOPOLE AT THE EDGE OF A WIRE-GRID BOX, BASE SEGMENT FEED

FREQUENCY GHZ.	AV. POWER GAIN	IMPEDANCE/ ADMITTANCE
1.0 GHZ.	1.17	28.9-j45.8 9.90+j15.6
1.05 GHZ.	1.10	31.4-j30.8 16.2+j16.0
1.1 GHZ.	1.08	34.4-j16.0 24.0+j11.1
1.15 GHZ.	1.11	38.1-j1.08 26.2+j0.74
1.2 GHZ.	1.18	43.0+j13.5 21.2-j6.67
1.3 GHZ.	1.40	55.4+j41.0 11.7-j8.63
1.4 GHZ.	1.65	71.1+j65.7 7.60-j7.00

TABLE 4

CALCULATED DATA FOR A MONOPOLE AT THE CORNER OF A WIRE-GRID BOX, BASE SEGMENT FEED

FREQUENCY GHZ.	AVG. POWER GAIN	IMPEDANCE/ ADMITTANCE
1.0 GHZ.	1.86	48.0-j47.4 10.6+j10.4
1.05 GHZ.	1.86	49.9-j34.5 13.7+j9.37
1.1 GHZ.	1.87	52.0-j6.63 16.6+j6.61
1.15 GHZ.	1.87	55.3-j6.63 17.8+j2.13
1.2 GHZ.	1.87	60.1+j7.60 16.4-j2.07
1.3 GHZ.	1.88	74.3+j34.6 11.1-j5.10
1.4 GHZ.	1.88	92.7+j55.0 8.00-j4.73

6 CM. MONOPOLE AT CENTER OF SURFACE PATCH BOX

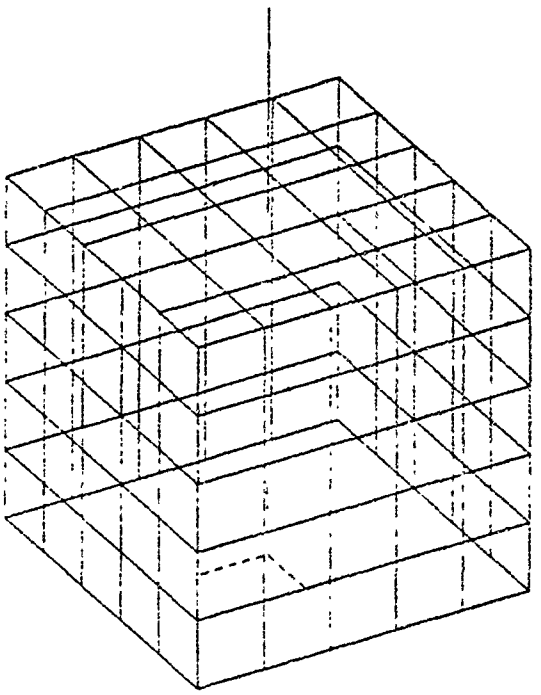

THETA = 60.00 PHI = 60.00 ETA = 90.00

Figure 3.6 6 cm. Monopole at Center of Surface-Patch Box.

6 CM. MONOPOLE AT EDGE 3.5 CM. FROM CENTER

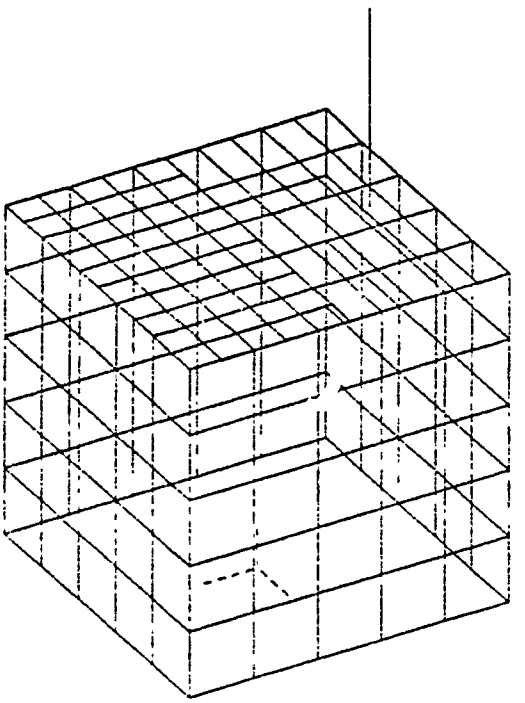

THETA = 60.00 PHI = 60.00 ETA = 90.00

Figure 3.7 6 cm. Monopole at Edge 3.5 cm. from Center.

6 CM. MONOPOLE AT CORNER4.93 CM. FROM CENTER

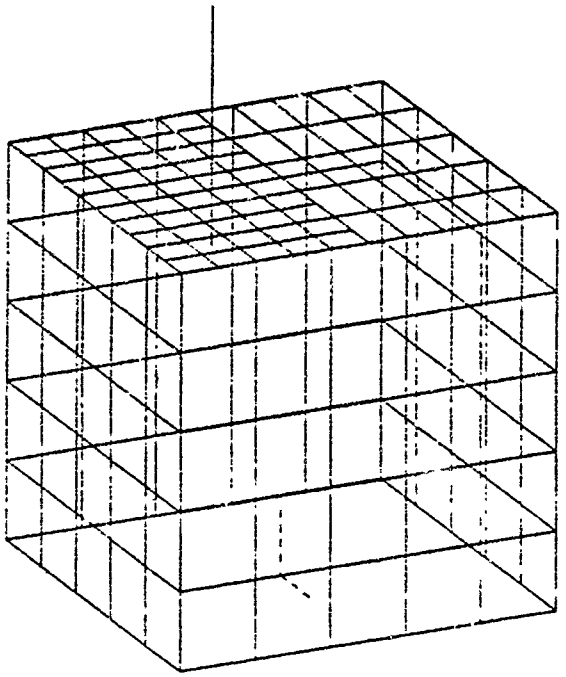

THETA = 70.00 PHI = 65.00 ETA = 90.00

Figure 3.8 6 cm. Monopole at Corner 4.93 cm. from Center.

TABLE 5

CALCULATED DATA FOR A MONOPOLE AT THE CENTER OF A SURFACE-PATCH BOX, BASE SEGMENT FEED

FREQUENCY GHZ.	AVG. POWER GAIN	IMPEDANCE/ ADMITTANCE
1.00 GHZ.	2.02	10.8-j20.2 20.6+j38.4
1.05 GHZ.	2.01	14.3-j5.49 60.6+j23.2
1.10 GHZ.	2.01	18.8+j8.58 43.9-j19.9
1.15 GHZ.	2.01	24.2+j21.9 22.7-j20.0
1.175 GHZ.	2.01	27.3+j28.2 17.1-j18.2
1.2 GHZ.	2.01	30.6+j34.2 14.5-j16.1
1.225 GHZ.	2.01	34.0+j40.0 12.3-j14.5
1.30 GHZ.	2.01	44.8+j55.5 8.84-j10.9
1.4 GHZ.	2.02	58.4+j71.8 6.81-j8.37

TABLE 6

CALCULATED DATA FOR A MONOPOLE AT THE EDGE OF A SURFACE-PATCH BOX, BASE SEGMENT FEED

FREQUENCY GHZ.	AVG. POWER GAIN	IMPEDANCE/ ADMITTANCE
1.00 GHZ.	1.92	22.6+j7.40 39.0-j13.1
1.05 GHZ.	1.92	25.3+j18.4 25.9-j18.8
1.10 GHZ.	1.92	28.3+j29.4 16.9-j17.5
1.15 GHZ.	1.88	32.9+j40.0 12.1-j14.8
1.175 GHZ.	1.88	35.2+j46.0 10.4-j13.7
1.2 GHZ.	1.88	37.6+j51.5 9.23-j12.6
1.225 GHZ.	1.88	40.3+j57.0 8.77-j11.7
1.3 GHZ.	1.89	49.5+j72.3 6.44-j9.41
1.4 GHZ.	1.89	123.+j220. 1.94-j3.46

TABLE 7

CALCULATED DATA FOR A MONOPOLE AT THE CORNER OF A SURFACE PATCH BOX, BASE SEGMENT FEED

FREQUENCY GHZ.	AV. POWER GAIN	IMPEDANCE/ ADMITTANCE
1.00 GHZ.	1.85	34.1-j53.2 8.52+j13.3
1.05 GHZ.	1.86	36.2-j40.5 12.2+j13.7
1.10 GHZ.	1.87	38.7-j20.4 17.0+j12.1
1.15 GHZ.	1.83	43.0-j14.2 20.9+j6.93
1.175 GHZ.	1.83	45.1-j7.38 21.5+j3.52
1.20 GHZ.	1.83	47.6-j.622 21.0+j.270
1.225 GHZ.	1.83	50.4+j6.01 19.5-j2.33
1.3 GHZ.	1.83	60.6+j24.7 14.1-j5.70
1.4 GHZ.	1.82	77.4+j45.9 9.54-j5.66

IV. WIRE GRID SOURCE BOX

The results of the average power gain and input impedance of the wire-grid cube-shaped box model are displayed in Table 8. For all of the frequencies chosen, the average power gain was close to one. (This model was in free space where the theoretical average power gain must be one). Only input impedance values for frequencies from 42 to 450 MHz can be considered useable because the ratios of the real part to the imaginary part are less than 10^4. For frequencies of 150 and 300 MHz, where the side dimension of the box is one and one-half wavelength, respectively, the ratio of the real part to the imaginary part was 10^0, which indicates that the dipole is resonant ($\lambda/2$ and λ long) and radiates very well through the widely-spaced wire grids. However when the model gets smaller in relation to the wavelength, as for 30 MHz and below, the results have ratios of 10^4 and higher between the real and the imaginary parts of the input impedance.

Calculations of the electrical near field for the frequencies of 30, 75 and 300 MHz, were performed for a path starting at the interior dipole and passing through the wire grid to the outside of the box, (see Figures 4.1 and 4.2 and Appendix A). The plots show the E field along the Y and Z axis. It can be seen in all the plots that the fields

inside the box at the wire grid walls are down several orders of magnitude from those at the dipole's surface. Passing through the grid, the fields drop suddenly by another order of magnitude for the two lower frequencies. At 300 MHz, where the grid spacing is very wide ($.4\lambda$) the box is quite transparent, with little shielding effect.

TABLE 8

CALCULATED DATA FOR THE DIPOLE INSIDE
THE WIRE-GRID BOX

FREQUENCY Mhz.	LAMBDA Mts.	AV. POWER GAIN	IMPEDANCE
3	100	.98	$.88\ 10^{0} - j.22\ 10^{5}$
7.5	40	.98	$.53\ 10^{-2} - j.90\ 10^{4}$
15	20	.98	$.18\ 10^{-1} - j.45\ 10^{4}$
30	10	.99	$.41\ 10^{-2} - j.21\ 10^{4}$
35	8.57	.97	$.11\ 10^{-1} - j.18\ 10^{4}$
42	7.14	.97	$.22\ 10^{0} - j.15\ 10^{4}$
50	6	.98	$.99\ 10^{0} - j.12\ 10^{4}$
62	4.83	.98	$.47\ 10^{1} - j.89\ 10^{3}$
75	4	.98	$.33\ 10^{2} - j.62\ 10^{3}$
92	3.26	.98	$.74\ 10^{2} - j.54\ 10^{3}$
110	2.72	.98	$.19\ 10^{2} - j.30\ 10^{3}$
150	2	.98	$.53\ 10^{2} + j.33\ 10^{2}$
300	1	.97	$.18\ 10^{4} + j.12\ 10^{4}$
450	.66	.97	$.12\ 10^{3} + j.60\ 10^{2}$

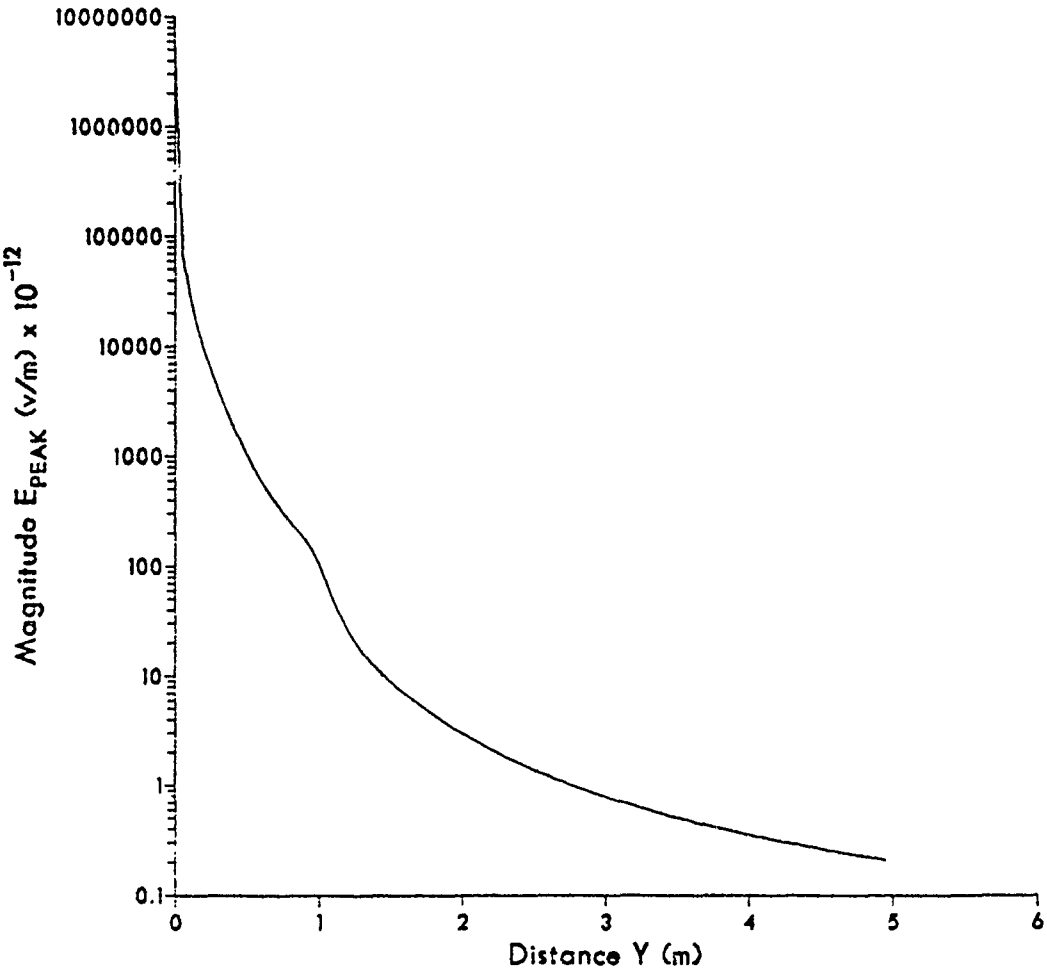

Figure 4.1 E-Field along Dipole Axis (Z-Axis) for 1M. Dipole inside 2M. Wire-Grid Box at 30 MHz.

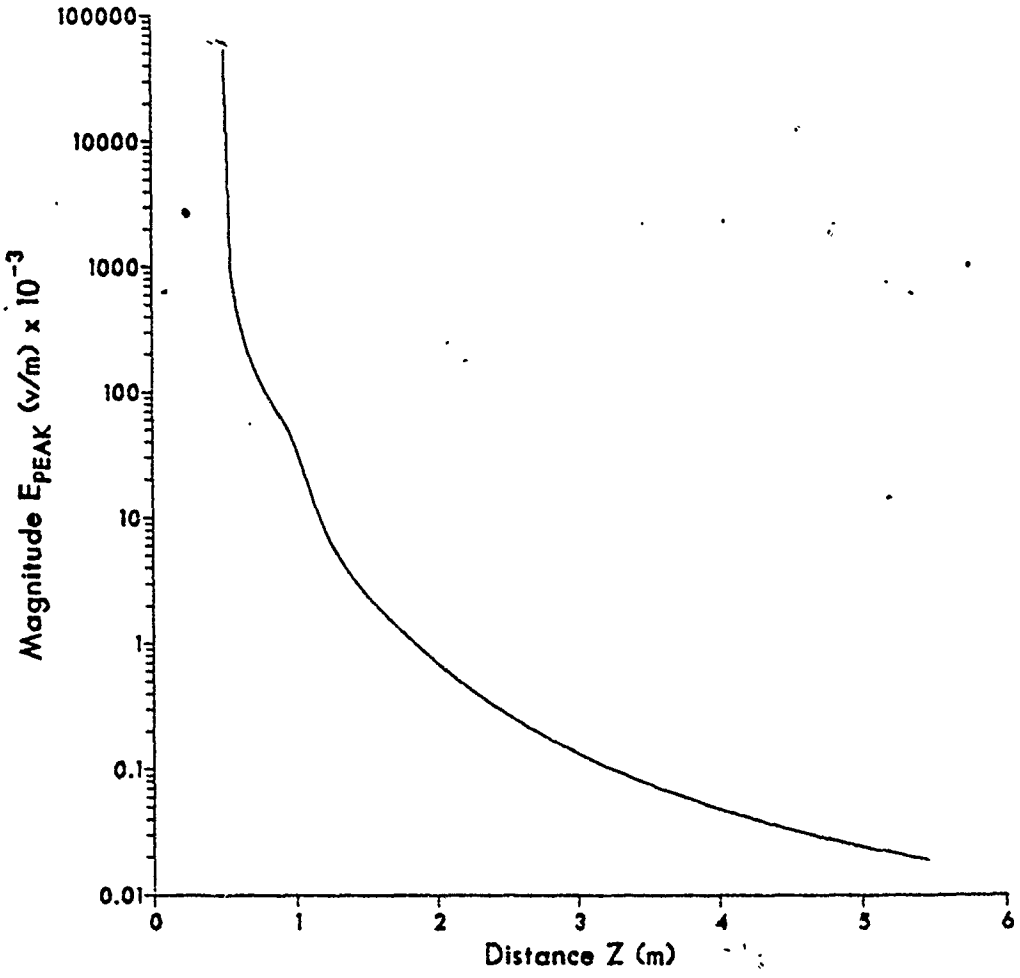

Figure 4.2 E-Field perpendicular to Dipole Axis (Y-Axis) for 1M. Dipole inside 2M. Wire Grid Box at 30 MHz.

V. RESULTS OF THE VARIATION OF THE POSITION OF THE MONOPOLE ON THE BOX

A. WIRE GRID CASE

To describe the curves which show the measurements and the calculation of the input impedance for the variation of the position of the 6 cm. monopole, five composite graphs were constructed showing the curves of NEC-calculated and measured Conductance (G) and Susceptance (B) from Reference 2, (see Figures 5.1 through 5.5). In the case of the monopole at the center of the box, the resonant frequency, as defined by the axis crossing of the susceptance curve, decreased from 1.138 to 1.125 GHz for Figure 5.1 (base segment feed), decreased from 1.138 to 1.122 GHz for Figure 5.2 (second segment feed), and decreased from 1.138 to 1.123 GHz for Figure 5.3 (the average of the two different feed methods). All these are relative to the measured susceptance from Reference 2. The variation was small due to the feed position. The feed segment was varied only for this position of the monopole. In some cases, when the feeding segment is tied to many other segments, errors may result. When feeding a vertical segment tied to four horizontal segments, calculations are difficult because the segments which are fed usually like to have a straight segment on both sides. Due to the good results obtained with the base segment feed, all the other comparisons are with the

monopole base segment feed; the measured data was also obtained by feeding that segment. The peak of the real part of the input admittance was lower for the calculated value, changing from 46.4 to 41 mS.

In the case of the monopole at the edge of the box, the calculated resonant frequency decreased slightly from 1.164 to 1.155 GHz and the peak conductance varied from 31.7 to 26.2 mS (Figure 5.4) in comparison to measurements. In the case of the monopole at the corner, the NEC resonant frequency decreased from 1.192 to 1.157 GHz and the peak conductance from 20.9 to 17.8 mS (Figure 5.5). For this wire-grid model, the results of the calculated data are very close to the measured values from Reference 2. Also, the result of the average power gain for this model were close to two (correct value of average power gain for perfect conducting ground plane).

B. SURFACE-PATCH CASE

For this model, the results of the calculated (NEC) input admittance were very good for the monopole located at the corner. There was a shift in resonant frequency of about -5 % for the monopole at center, (see Figure 5.6). For the edge-mounted geometry, the correlation between measurement and calculation was quite poor (see figure 5.7). The calculated values of the average power gain were close to two for all positions of the monopole (see Tables 5, 6, and 7, Chapter III). For the monopole at the center of the

surface-patch box, the resonant frequency decreased from 1.138 to 1.052 GHz and the peak conductance increased from 46.4 to 60.6 mS (see Figure 5.6). The resonant frequency for corner mounting changed from 1.192 to 1.2 GHz and the peak conductance increased from 20.9 to 21.5 mS (see Figure 5.8). This accuracy might be due to the fact that in this case the top of the surface-patch box had been more finely divided into smaller patches than for the other two mounting cases. This was done in order to position the monopole at a specific distance from the center, close to the distance used in Reference 2.

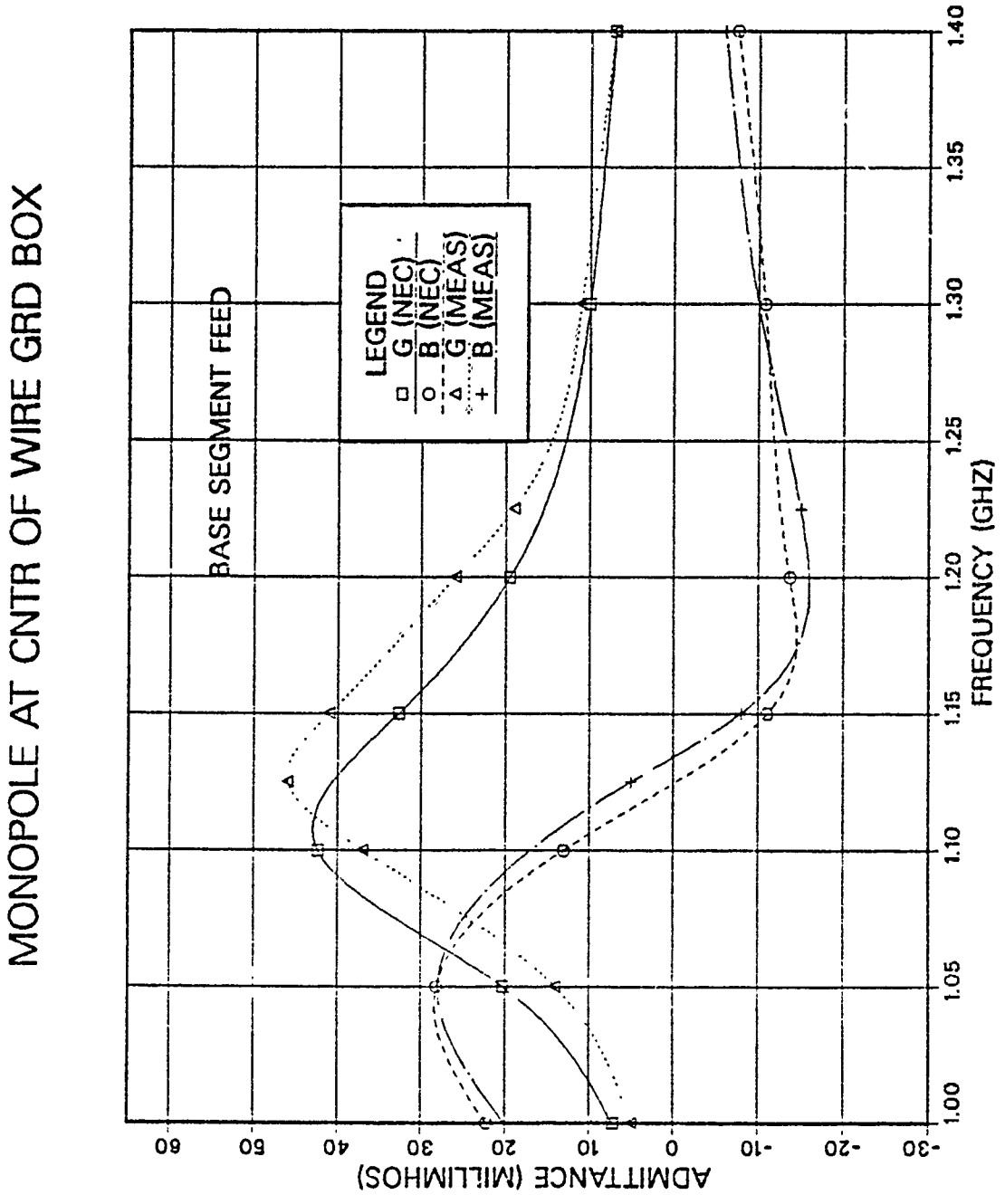

Figure 5.1 6 cm. Monopole at center of Wire-Grid Box, Base Segment Feed.

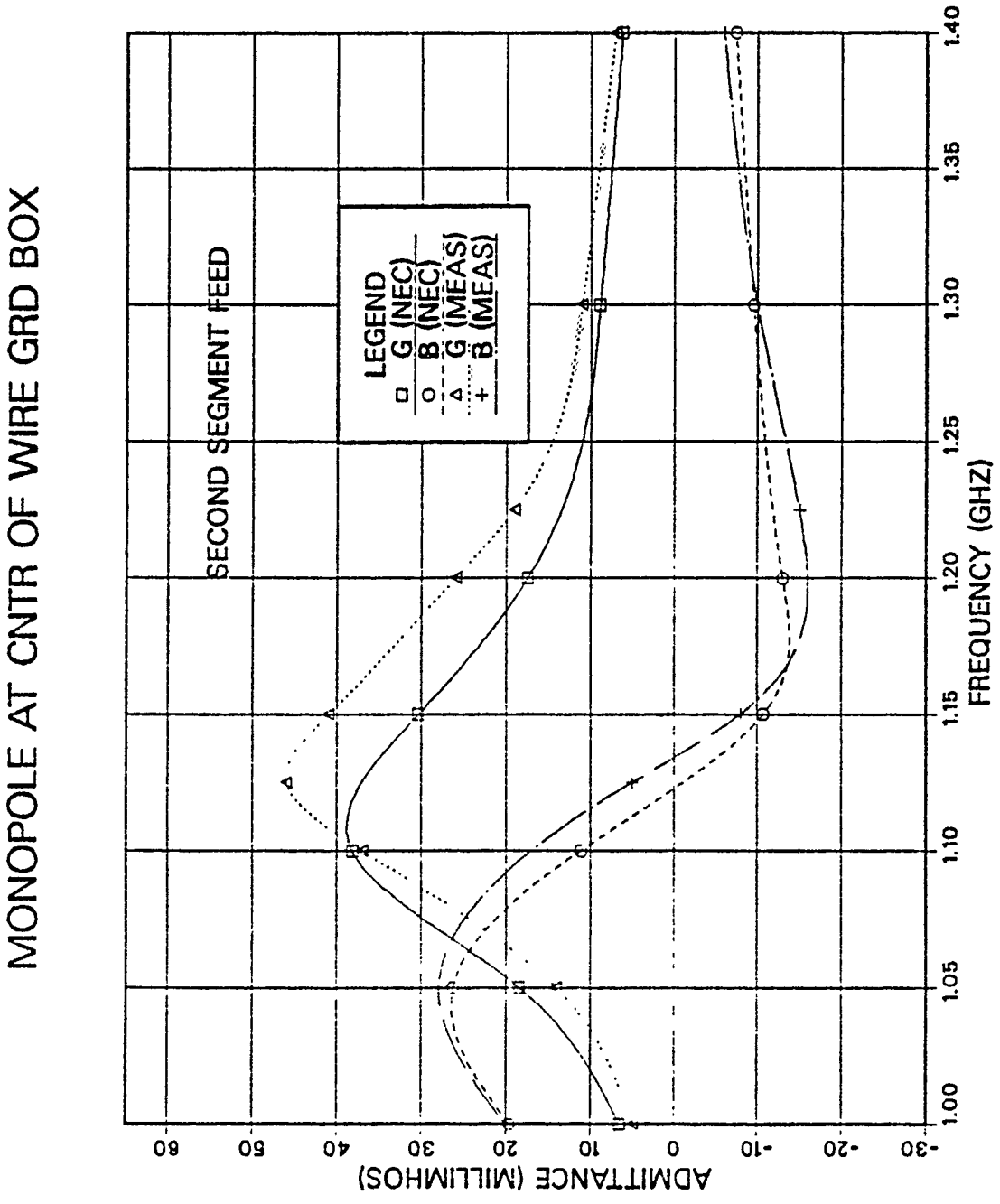

Figure 5.2 6 cm. Monopole at center of Wire-Grid Box, Second Segment Feed.

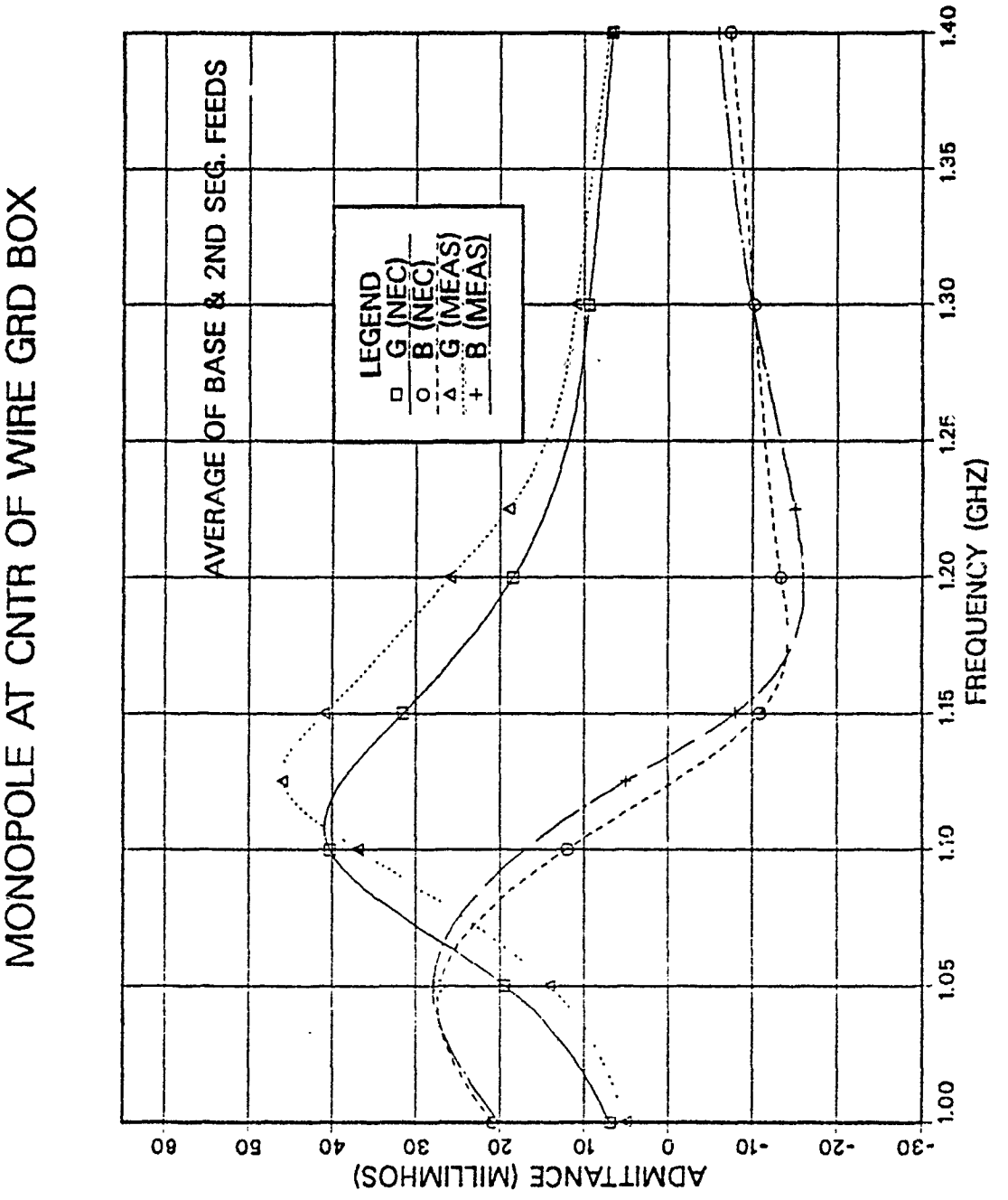

Figure 5.3 6 cm. Monopole at center of Wire-Grid Box, Average of Base and second Segment Feeds.

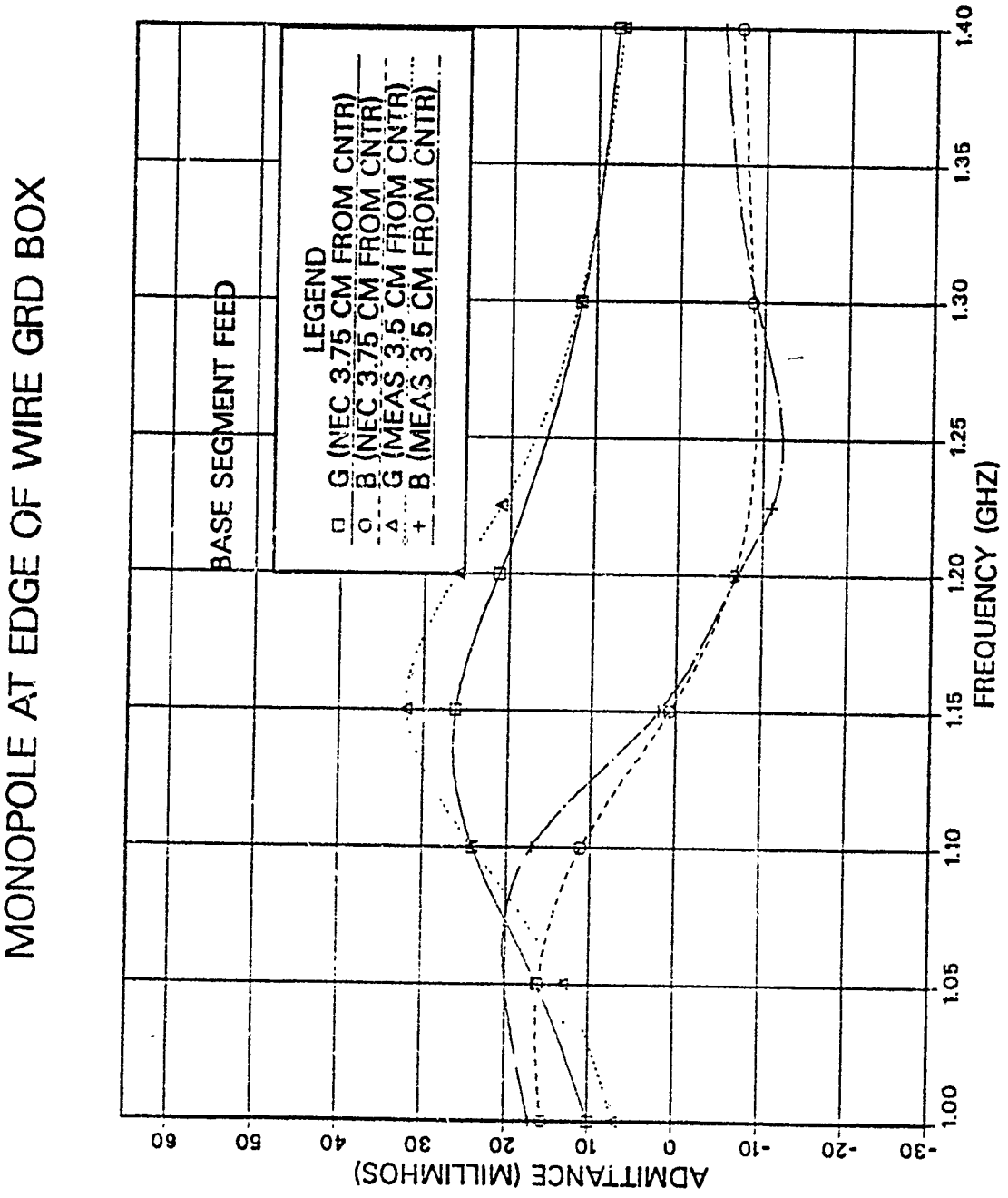

Figure 5.4 6 cm. Monopole at Edge of Wire-Grid Box, Base Segment Feed.

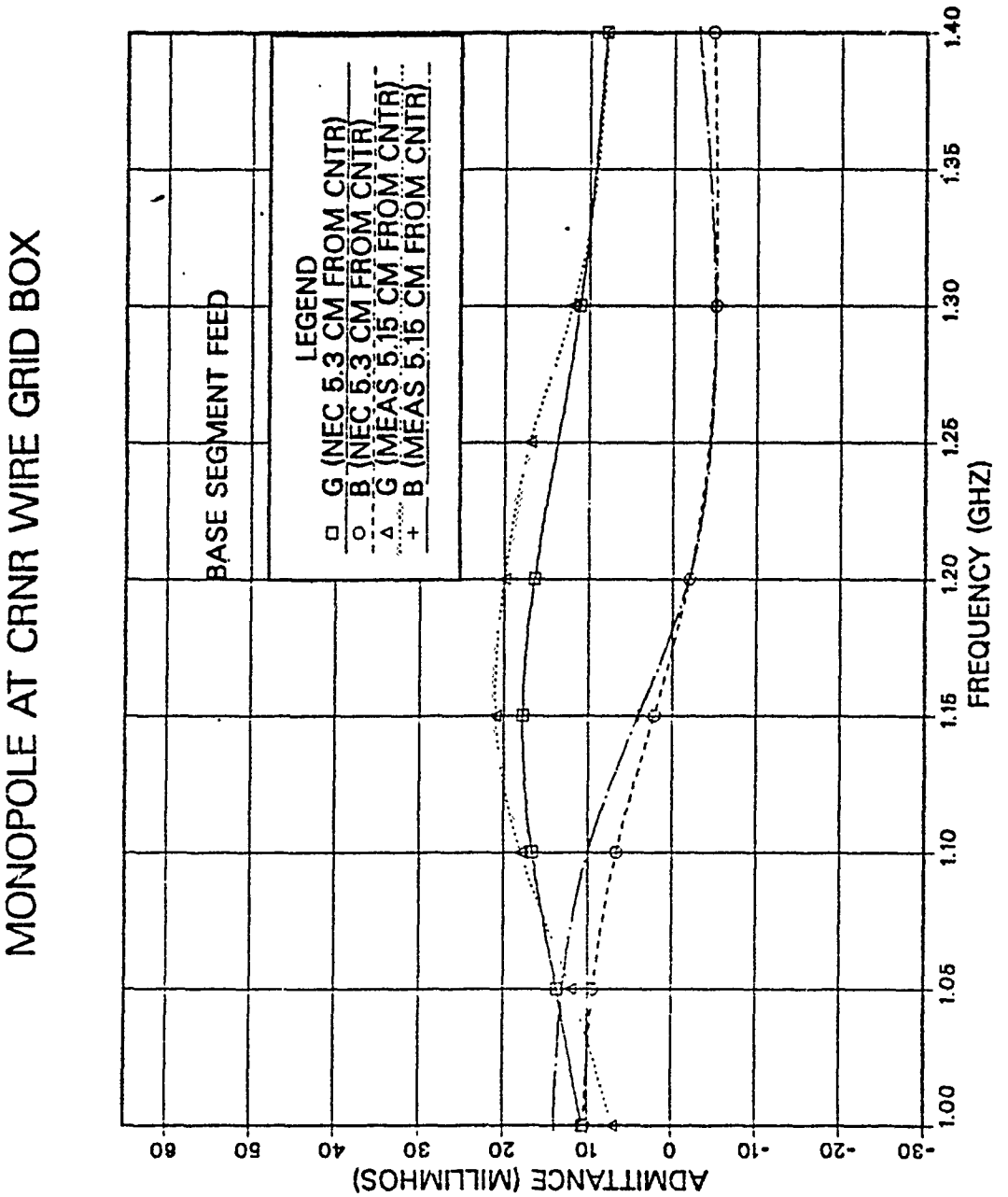

Figure 5.5 6 cm. Monopole at Corner of Wire-Grid Box, Base Segment Feed.

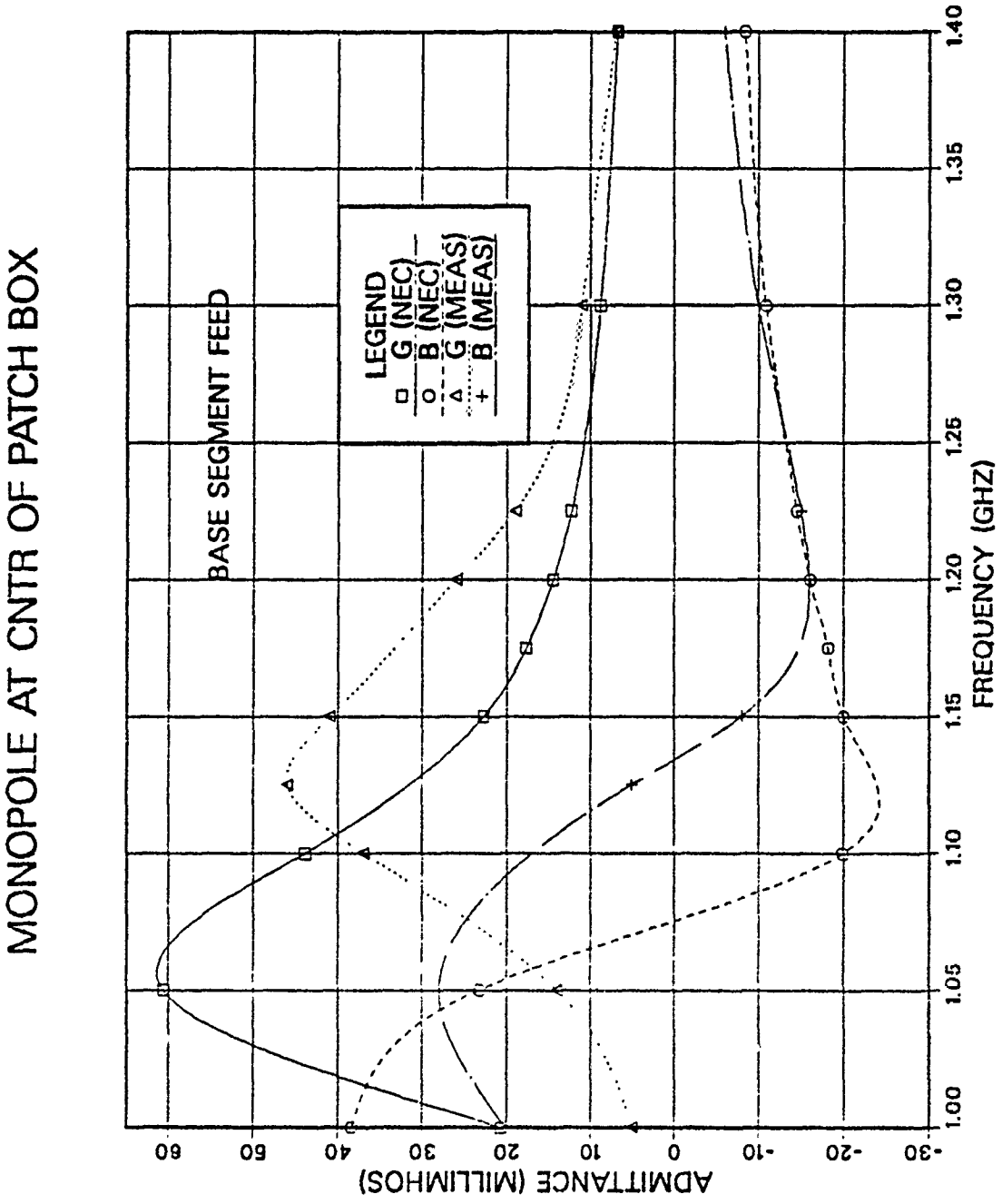

Figure 5.6 6 cm. Monopole at Center of Surface-Patch Box, Base Segment Feed.

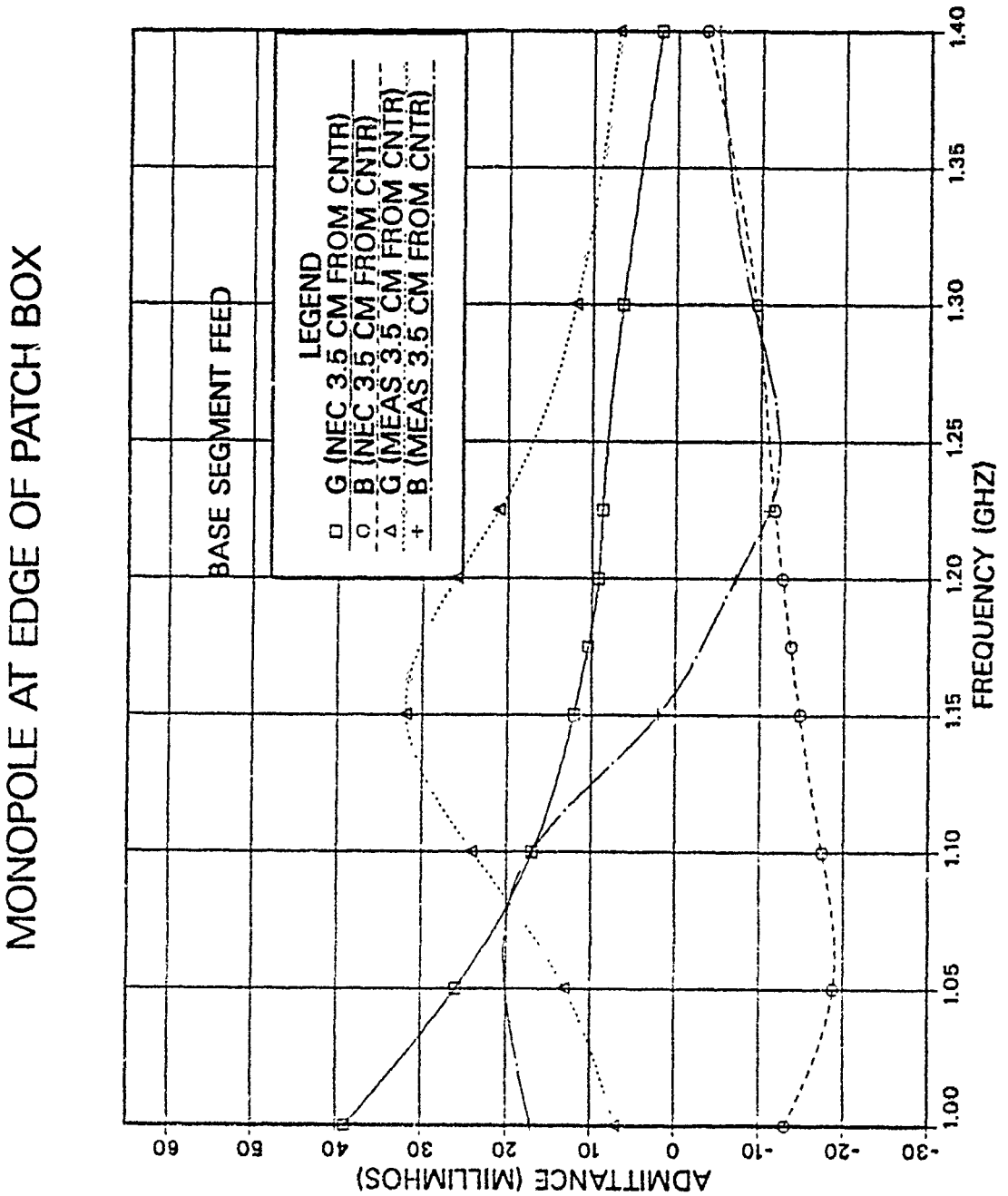

Figure 5.7 6 cm. Monopole at Edge of Surface-Patch Box, Base Segment Feed.

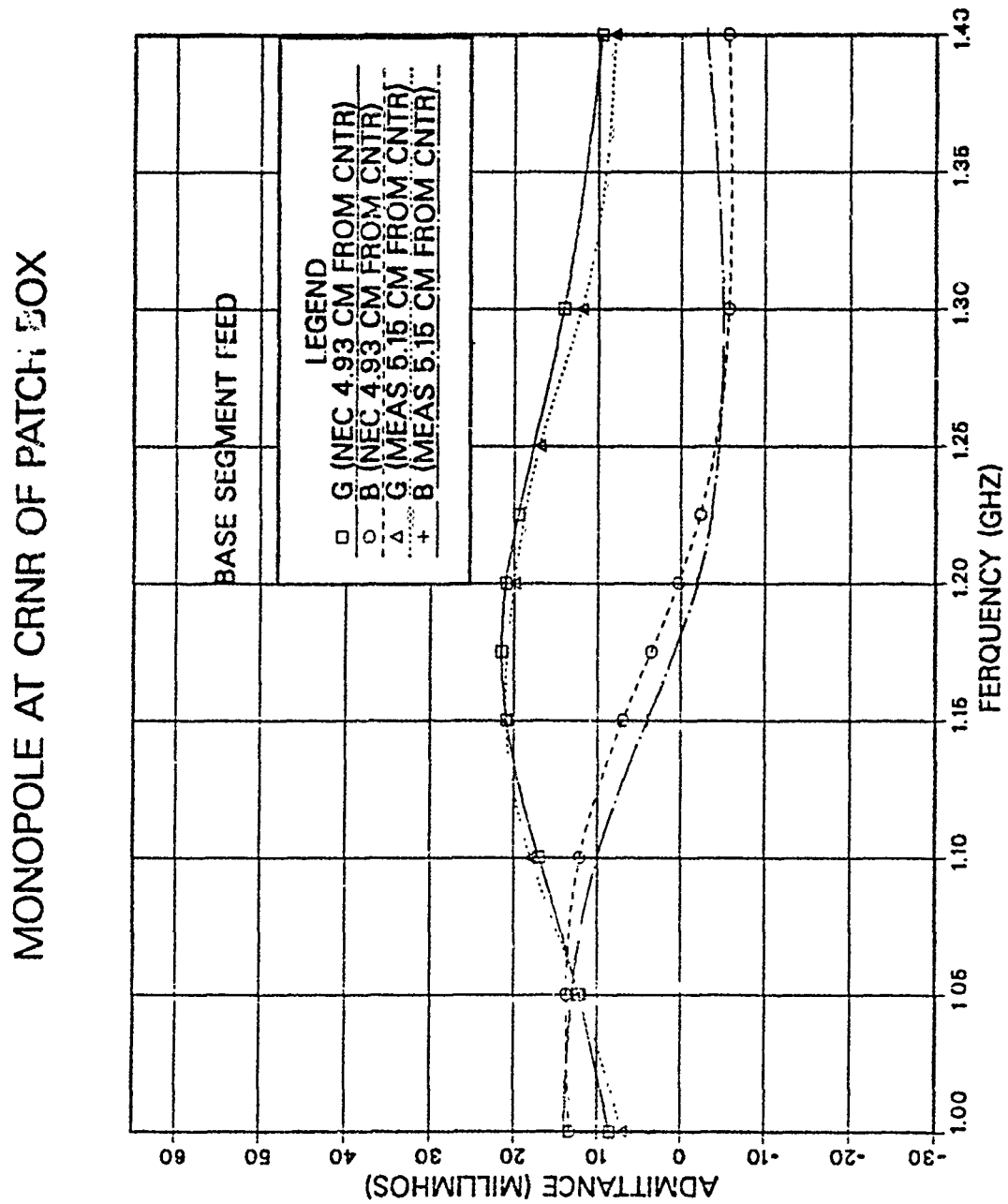

Figure 5.8 6 cm. Monopole at Corner of Surface-Patch Box, Base Segment Feed.

VI. CONCLUSION AND RECOMMENDATIONS

The initial goal of this work was to investigate the accuracy of near-field calculations using the Numerical Electromagnetic Code (NEC) on ship-like structures. Since no validation bench mark results were available for ship antenna installations, a modeling exercise was undertaken, which would yield insight for near-field work in the future. Box-like structures were analyzed, one with an interior dipole and one with a monopole mounted on the top. For the dipole inside the wire grid, there were no measured values to compare to, but the calculations of the average power gain and input impedance were as expected. The E field variation was also examined as a function of frequency. The fields inside the box drop off as the observation point moves away from the source. For a non-radiating structure, the fields would be similar to the interior of a small cavity, with standing wave patterns. Any input resistance in the perfect cavity case could only come from dipole conductor loss. The leaky nature of the wire box produced non-zero input resistance for the dipole, but as the frequency was lowered to a point where the grid size approacned $\lambda/20$, the real part of the input impedance was numerically swamped out by the reactance, an expected result arising from less radiation leakage. The value of the leaky

box model is that it raises concerns about wire grids used as models of ships structures for **HF RADHAZ** predictions. On a real-world ship, the antennas/sources will be located on the exterior of the ship. The predicted near fields around these radiators may be subjected to substantial calculation errors if the wire grid surfaces are not "tight" enough. Measurements of near-fields for well-controlled generic shipboard shapes are needed as a validation benchmark for additional numerical model developments.

In the case of the monopole over the cube-shaped box, the two modeling methods that NEC has available were tried. The wire-grid model worked very well, but the surface patch gave good results only for the monopole positioned at the corner of the box where the patches at the top are smaller. If smaller patches (finer surface current definition) for the other two positions of the monopole had been used the results might have been better. Those data sets are easy to produce, but will be difficult to calculate because of excessive computer time requirements. It is recommended that this be done on a super-computer in the continuation of this work.

This study is an important step in the direction of near-field modeling of shipboard shapes because it shows the kind of wire-grid definition needed to get accurate input impedance for antennas on boxes and gives an idea of how to apply surface-patch modeling for accurate input impedance.

APPENDIX A

PLOTS OF E-FIELDS ALONG DIPOLE AXIS (Z-AXIS) AND PERPENDICULAR AXIS (Y-AXIS) FOR 1M DIPOLE INSIDE WIRE GRID BOX

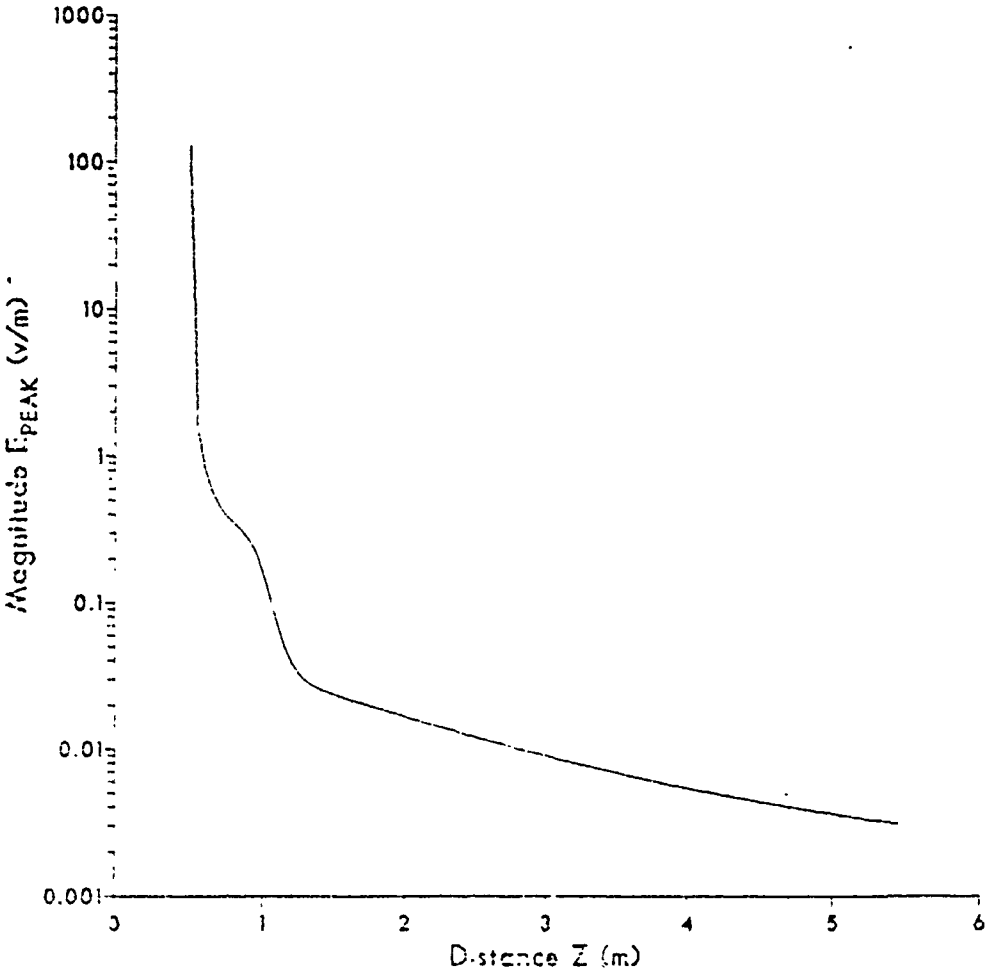

Figure A.1 E-Field Along Dipole Axis (Z-Axis) for 1M. Dipole Inside 2M. Wire Grid Box at 75 MHz.

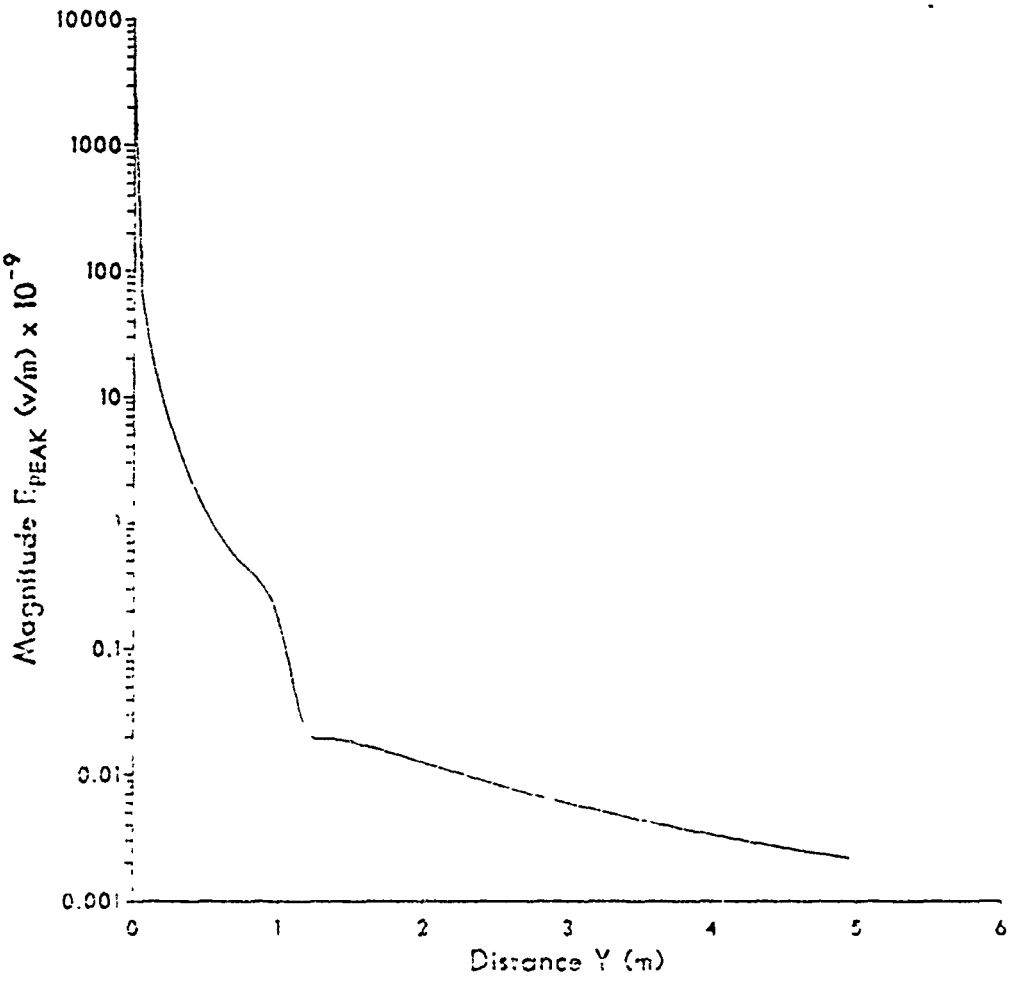

Figure A.2 E-Field Perpendicular to Dipole Axis (Y-Axis) For 1M. Dipole Inside 2M. Wire Grid Box at 75 MHz.

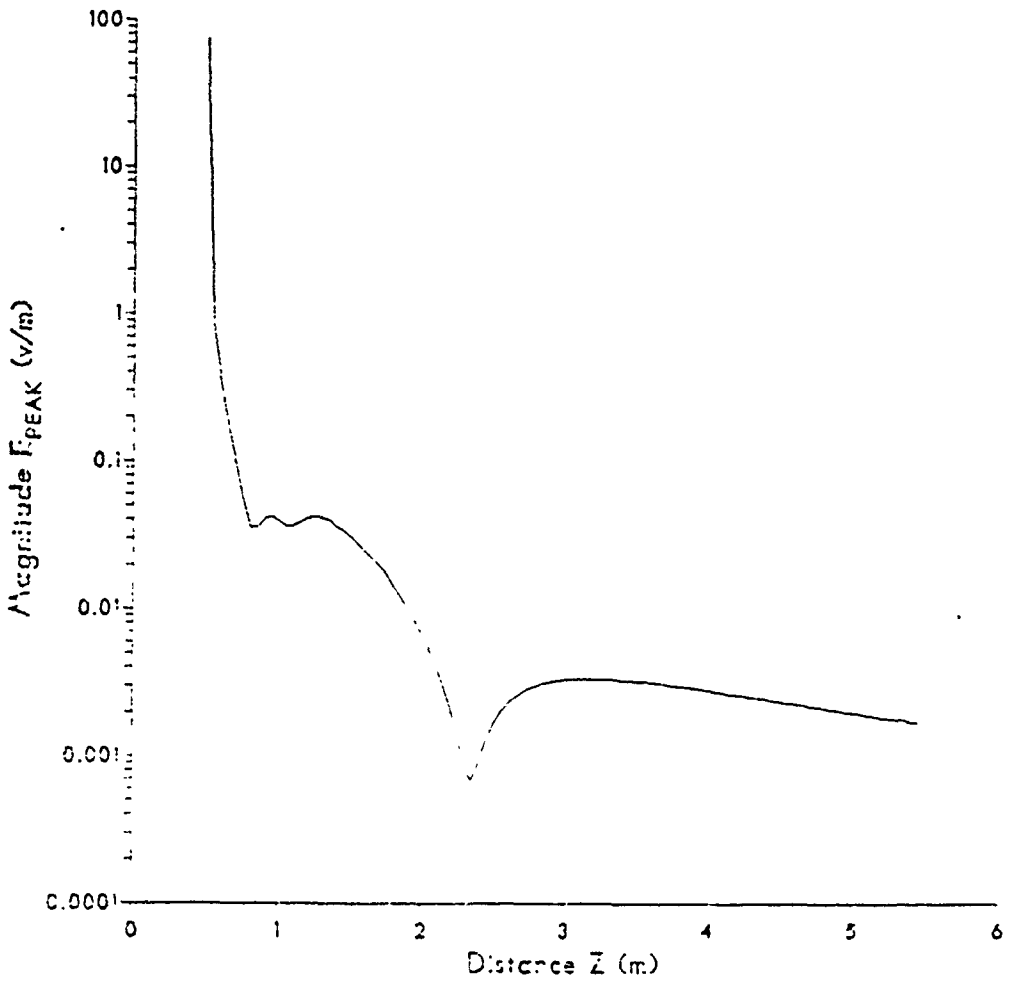

Figure A.3 E-Field Along Dipole Axis (Z-Axis) for 1M. Dipole Inside 2M. Wire Grid Box at 300 MHz.

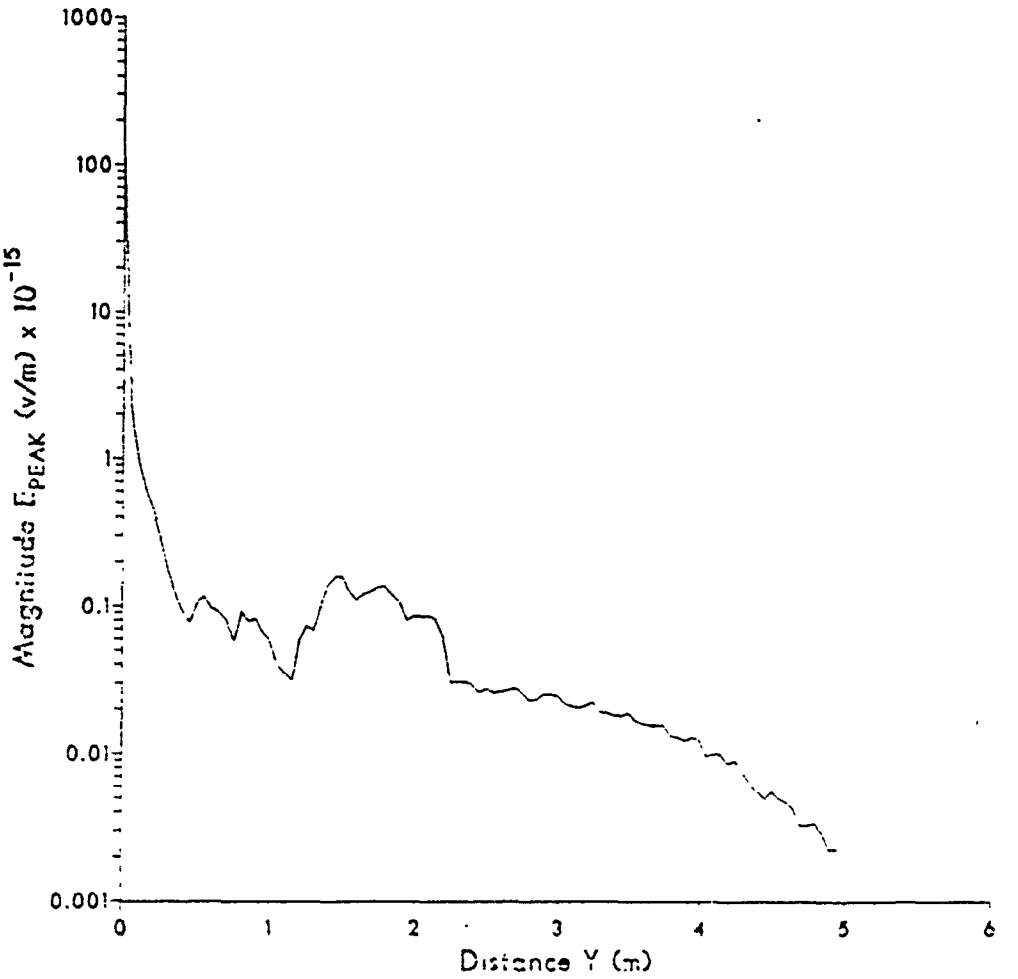

Figure A.4 E-Field Perpendicular to Dipole Axis (Y-Axis) for 1M. Dipole Inside 2M. Wire Grid Box at 300 MHz.

APPENDIX B
INPUT DATA FILES

```
CM WIRE GRID 10 CM. LONG
CM CELLS .125 X.125 GROUND
CE
GW 100,4,.5,-.5,1,0,-.5,1,.01
GM 1,7,0,0,0,0,0,-.125,100.100
GW 200,8,.5,-.5,1,.5,-.5,0,.01
GM 2,3,0,0,0,0,.125,0,200.201
GM 3,3,0,0,0,-.125,0,0,200.201
GW 300,4,.5,-.5,1,.5,0,1,.01
GM 4,7,0,0,0,0,0,-.125,300.303
GW 400,4,.5,-.375,1,0,-.375,1,.01
GM 5,2,0,0,0,0,.125,0,400.404
GW 500,4,.375,-.5,1,.375,0,1,.01
GM 6,2,0,0,0,-.125,0,0,500.505
GX 0,110
GS 0,0,.1
GE 1
FR 0,0,0,0,1000
GN 1
WG
XQ 0
EN
```

1. Data File for Wire-Grid Box.

```
CM 6 CM. MONOPOLE AT CENTER OF WIRE GRID FREQ 1.0 GHZ
CM CALCULATE OF AVERAGE GAIN AND IMPUT IMPEDANCE
CE
GW 2,8,0,-.5,1,0,.5,1,.01
GW 3,8,.5,0,1,-.5,0,1,.01
GW 1,5,0,0,1,0,0,1.6,.016
GS 0,0,.1
GE 1
EX 0,1,1,0,1,0
RP 0,31,4,1002,0,0,3,15
NO 0
EN
```

2. Data File 6 cm. Monopole at Center Wire Grid Box.

```
CM 6 CM. MONOPOLE AT EDGE OF WIRE GRID FREQ 1.0 GHZ
CM CALCULATE OF AVERAGE GAIN AND IMPUT IMPEDANCE
CE
GF
GW 2,8,0,-.5,1,0,.5,1,.01
GW 3,8,.5,0,1,-.5,0,1,.01
GW 1,5,-.375,0,1,-.375,0,1.6,.016
GS 0,0,.1
GE
EX 0,1,1,0,1,0
RP 0,31,13,1002,0,0,3,15
XQ 0
EN
```

3. Data File 6 cm. Monopole at Edge Wire-Grid Box.

```
CM 6 CM. MONOPOLE AT CORNER OF WIRE GRID FREQ 1.0 GHZ
CM CALCULATE OF AVERAGE GAIN AND IMPUT IMPEDANCE
CE
GF
GW 2,8,0,-.5,1,0,.5,1,.01
GW 3,8,.5,0,1,-.5,0,1,.01
GW 1,5,.375,.375,1,.375,.375,1.6,.016
GS 0,0,.1
GE
EX 0,1,1,0,1,0
RP 0,31,13,1002,0,45,3,15
XQ 0
EN
```

4. Data File 6 cm. Monopole at Corner-Wire Grid Box.

```
CE SURFACE PATCH  GROUND  FREQ. 1.0GHZ
SM 3,3, .5,-.5,0, .5,-.5,1
SC 0,0, 0,-.5,1
SM 3,3, .5,-.5,0, .5,0,0
SC 0,0, .5,0,1
GX 0,110
SM 5,5, -.5,-.5,1, .5,-.5,1
SC 0,0, .5,.5,1
GS 0,0,.1
GE 1
FR 0,0,0,0,1000
GN 1
WG
XQ 0
EN
```

5. Data File Surface-Patch Box for Monopole at Center.

```
CE SURFACE PATCH  GROUND
SM 3,3, .5,-.5,0, .5,-.5,1
SC 0,0, 0,-.5,1
SM 3,3, .5,-.5,0, .5,0,0
SC 0,0, .5,0,1
GX 0,110
SM 5,5, -.5,.5,1, -.5,-.5,1
SC 0,0, 0,-.5,1
SM 10,5, 0,.5,1, 0,-.5,1
SC 0,0, .5,-.5,1
GS 0,0,.1
GE 1
FR 0,0,0,0,1000
GN 1
WG
XQ 0
EN
```

6. Data File Surface-Patch Box for Monopole at Edge and Corner.

```
CM 6 CM. MONOPOLE AT CENTER SURFACE PATCH  FREQ 1.0 GHZ
CM CALCULATE OF AVERAGE GAIN AND IMPUT IMPEDACE.
CE
GF
GW 1,5,0,0,1,0,0,1.6,.016
GS 0,0,.1
GE
EX 0,1,1,0,1,0
RP 0,31,4,1002,0,0,3,15
XO 0
EN
```

7. Data File for 6 cm. Monopole at Center Surface-Patch Box.

```
CM 6 CM. MONOPOLE AT EDGE SURFACE PATCH  FREQ 1.0 GHZ
CM CALCULATE OF AVERAGE GAIN AND IMPUT IMPEDACE.
CE
GF
GW 1,5,-.35,0,1,-.35,0,1.6,.016
GS 0,0,.1
GE
EX 0,1,1,0,1,0
RP 0,31,13,1002,0,0,3,15
XO 0
EN
```

8. Data File for 6 cm. Monopole at Edge Surface Patch.

```
CM MONOPOLE 6CM. AT CORNER SURFACE PATCH  FREQ 1.0 GHZ
CM CALCULATE OF AVERAGE GAIN AND IMPUT IMPEDACE.
CE
GF
GW 1,5,.35,.35,1,.35,.35,1.6,.016
GS 0,0,.1
GE
EX 0,1,1,0,1,0
RP 0,31,13,1002,0,45,3,15
XO 0
EN
```

9. Data File for 6 cm. Monopole at Corner Surface Patch.

```
CM AVERAGE GAIN DIPOLE IN A WIRE GRID
CM CELLS .4X.4 DIPOLE LENGTH 1Z FREE SPACE
CE
GW 100,1,1,-1,1,0,-1,1,.04
GM 1,2,0,0,0,0,.4,0,100.100
GM 1,2,0,0,0,0,0,-.4,100.100
GW 200,1,1,-1,1,1,0,1,.04
GM 2,2,0,0,0,-.4,0,0,200.200
GM 2,2,0,0,0,0,0,-.4,200.200
GW 300,1,1,-1,1,1,-1,0,.04
GM 3,2,0,0,0,-.4,0,0,300.300
GM 3,2,0,0,0,0,.4,0,300.300
GX 0,111
GE
FR 0,0,0,0,15
WG
EN
```

```
CM DIPOLE IN WIRE GRID AT 0,0,-.5  0,0,.5
CM FREQ. 15 MHZ, CALCULATE AVERAGE GAIN, INPUT IMPEDANCE
CE
GW 1,5,0,0,-.5,0,0,.5,.001
GE
EX 0,1,3,0,1,0
RP 0,31,4,1002,0,0,3,15
XQ 0
EN
```

10. Data Files Wire-Grid Box 2 by 2 Meters
Dipole 1 Meters Long.

APPENDIX C

DESCRIPTION OF NEC

The Numerical Electromagnetics Code (NEC) is a user-oriented computer code for analysis of the electromagnetic response of antennas and other metal structures. It is built around the numerical solution of integral equations for the currents induced on the structure by sources or incident fields. This approach avoids many of the simplifying assumptions required by other solution methods and provides a highly accurate and versatile tool for electromagnetic analysis.

The code combines an integral equation for smooth surfaces with one specialized to wires to provide for convenient and accurate modeling of a wide range of structures. A model may include nonradiating networks and transmission lines connecting parts of the structure, perfect or imperfect conductors, and lumped element loading. A structure may also be modeled over a ground plane that may be either a perfect or imperfect conductor.

The excitation may be either voltage sources on the structure or an incident plane wave of linear or elliptic polarization. The output may include induced currents and charges, near electric or magnetic fields, and radiated fields. Hence, the program is suited to either antenna analysis or scattering and EMP studies.

The integral equation approach is best suited to structures with dimensions up to several wavelengths. Although there is no theoretical size limit, the numerical solution requires a matrix equation of increasing order as the structure size is increased relative to the wavelength. Hence, modeling very large structures may require more computer time and file storage than is practical on a particular machine. In such cases standard high-frequency approximations such as geometrical optics, physical optics, or geometrical theory of defraction may be more suitable than the integral equation approach used in NEC.

NEC contains the Numerical Green's Function for partitioned-matrix solution and a treatment for lossy grounds that is accurate for antennas very close to the ground surface. It also includes an option to compute maximum coupling between antennas and useful options for structure input.[Ref.6:p.1]

1. ZONING CONSIDERATIONS

NEC is a discrete sampling code where a complex structure must be discretized into a number of simple elements (wires or surface patches) to which the Electrical Field Integral Equation (EFIE) or Magnetic Field Integral Equation (MFIE) are applied. As with any description of the real world, there are approximations, but because of the versatility in modeling the geometry of a structure,

its approximations more closely resemble nature. The resemblance is strongly influenced by the choice of zoning (i.e., dissecting) the structure in the program. The smaller the geometric elements, the closer the model comes to reality. However, the smaller the elements, the larger number of elements, which means the larger the matrix of equations and hence, the more costly the solution. There is a point beyond which smaller zones do not yield a substantially more accurate solution; it may be necessary to rerun the problem with increasingly smaller elements to find the point of diminishing returns. The choice of proper zoning then is gained with experience and becomes as much of an art as it is a science. The guidelines for the science aspect are as follows.[Ref.6]

a. Wires

Segments should follow the paths of conductors using a piece-wise linear fit on curves. Generally, segments lengths (Δ) should be less than $.1\lambda$; shorter segments ($.05\lambda$) or less may be needed at critical regions (junctions or curves). Segments smaller than $10^{-3}\lambda$ should be avoided since the similarity of constant and cosine components lead to numerical inaccuracy. The radius of the wire (a) relative to λ depends on the Kernel use in the Integral Equation. Two options exist. The thin-wire Kernel models a filament current, while the extended Kernel models a uniform current distribution around the segment surface.

The fie[illegible] current is approximated by the
first [illegible]es expansion of the exact field, in
powers [illegible] (a^0) term is identical to the thin-
wire Ke[illegible] term extends the accuracy for larger
values [illegible] Kernels incorporate the thin-wire
approxi[illegible] require $2\pi a/\lambda \ll 1$. The thin-wire
Kernel [illegible]; the extended Kernel relaxes this
to Δ/a [illegible]ues ensure errors are less than 1%.
The ex[illegible] used at free wire ends and between
paralle[illegible]gments. The thin-wire Kernel is
always

b.

surface is modeled by small flat
surface conform as closely as possible to
curved [illegible]arameter defining a patch is a normal
unit v[illegible]ng from the [illegible] the patch,
defined coordinates. [illegible] must be
connect the patch center [illegible] program to
integra[illegible]urrent. The code [illegible] each patch
into f[illegible] about the wire end, along the unit
vector the surface of the of the patch. An
interpo is applied to the four patches to
represe the current onto the patches, and the
functio[illegible]y integrated. Patches with wires
connect[illegible]ve patches) should be chosen to be
approxi[illegible]h sides parallel to the unit vectors

defining the surface. Only one wire may connect to a patch, that wire may not be connected to another patch. A minimum of about 25 patches should be used per wavelength of surface area; the maximum size for an individual patch is about .04 square wavelength. The number of patches used increases, and the size of each patch decreases, as the radius of curvature decreases. Smaller patches should be used at edges since the current amplitude may vary rapidly in this region. Long narrow patches should be avoided. Patches are restricted to modeling voluminous bodies with closed surfaces; parallel surfaces on opposite sides cannot be too close together.

c. Ground Plane

For a perfectly conducting ground, the code generates a reflected image. Structures may be close to, or contact, the ground; however, for a horizontal wire: $\sqrt{h^2+a^2} > 10^{-6}\lambda$ where a = wire radius, h = height of wire axis above the ground plane, and $h/a \geq 3$.

A finitely conducting ground may be modeled by an image modified by the Fresnel Plane-wave Reflection coefficients. This method is fast, but of limited accuracy and should not be used for structures close to the ground, or having a large horizontal extent over the ground. The Sommerfeld/Norton model uses the exact solution and is accurate close to the ground; the horizontal restriction is the same as for a perfect ground. This model is only used

for wire to wire interactions, for surfaces the code reverts to Fresnel Reflection coefficients. [Ref. 6].

APPENDIX D

RADIATION HAZARD (RADHAZ) ON BOARD SHIPS

The near fields of Navy antennas are primarily important as radiation hazards **(RADHAZ)**. There are essentially three types of radiation hazards:

RADHAZ to Personnel (HERP)

RADHAZ to Ordnance (HERO)

RADHAZ to Fuel (HERF)

These hazards and their general near field criteria are discussed in the following sections.

a. Hazards of Electromagnetic Radiation to Personnel (HERP)

Most Navy platforms possess systems and equipment which radiate energy in some portion of the electromagnetic spectrum. The radiation can constitute a hazard for personnel. The degree to which personnel are exposed to the radiation depends on the type of platform, the systems installed, the location of the systems (particularly their antennas), the possibility of directive antennas illuminating areas occupied by personnel, etc.

The effects of exposure to this radiation can be classified into two categories, direct and indirect. Direct radiation is defined as the energy impinging directly on the body. Indirect radiation is defined as the capture of EM energy by a metallic object. Resulting voltage and currents cause burns when the metallic objects are contacted by personnel.

With certain reservations, physiologists generally agree that damage to personnel from direct radiation is primarily a heating effect.

In recent years, however, many distinctly nonthermal effects have been documented, some of which have been show to be dependent on peak powers whose average value is not great enough to produce heating. Frequency dependence, with no heating, has also characterized many of the observed effects. While the full significance of these effects as human hazards has not been established, the fact that they occur at average power levels considered to be negligible suggest that, at the least, an awareness of their existence should be assumed. Some recorded nonthermal effects listed in MIL-HDBK-238(NAVY) 1973 are:

(1) Minor changes in human blood properties upon exposure to EM energy of proper frequency and intensity.

(2) Auditory response. Certain people hear a buzz when exposed to microwave radiation. The sensation of sound is probably not the microwave frequency but response to the pulse repetition frequency.

(3) Abnormalities of the chromosome structure occurring upon exposure.

(4) Movement, orientation, and polarization of protein molecules in pulse RF fields.

(5) Unexplained response of man to radar. Epigastric distress, emotional upsets, and nausea may occasionally occur at as low as 5-10 mW/cm^2 and are most commonly associated with the frequency range from

$$8 \times 10^3 \text{ to } 12 \times 10^3 \text{ MHz}$$

Changes in the transport rate of materials across the blood-brain barrier in humans and animals have also been observed. The significance of these changes is not yet understood.

The Navy RADHAZ standard follows the current ANSI standard for 3 to 30 MHz with constant values below 3 MHz. Personnel shall not be exposed to a power density which, when averaged over any 0.1 hour period, exceeds $900/f^2$ (MHz) mW/cm^2 in the frequency domain of 3 to 30 MHz. Neither the root mean squared electric field strength (E) nor the root mean squared magnetic field strength (H) may exceed the following values when averaged over any 0.1 hour period:

$$E = \frac{1897}{f \text{ MHz}} \quad V/M$$

$$H = \frac{4.74}{f \text{ MHz}} \quad A/M$$

(These are the electric and magnetic field strengths roughly corresponding to electromagnetic waves in free space to which the value of power density show above may be assigned.) For a condition where exposure is not regular in

time or continuous in level over the 0.1 hour period, the equivalent energy fluence level of one-tenth of the power density number in units of $mW\text{-}h/cm^2$ may be use as the limit of exposure for any 0.1 hour period. In situations where measurements of two or more quantities are available, the most restrictive shall be used as the limiting factor.

RF burns constitute an indirect radiation effect. Ship communication transmitters induce voltages on various metallic structures such as underway replenishment gear, booms, and loading hooks. The voltages are capable of causing painful burns to personnel who come in contact with these structures.

It has been established that 140 volts or greater, measured from the object to ground, can cause burns to persons touching the object.

b. Hazards of Electromagnetic Radiation to Ordnance (HERO)

Hazards of electromagnetic radiation to ordnance (HERO) stem from the use of sensitive electroexplosive devices (EEDs) in ordnance systems. The principal emphasis is on protecting electroexplosive devices such as squibs, detonators, explosive switches, and ejection cartridges. Premature actuation of some of these devices can, of course, have dire consequences, such as rocket ignition or warhead detonation on a flight deck. Premature actuation by RF can also impact the reliability of a system, as for example when the power supply for a missile guidance system is expanded

inadvertently by the RF initiation of a squib switch. In addition, EED firing characteristics can be altered by electromagnetic induced heating.

For the above reasons NAVMAT Instruction 5101.1 requires that weapons systems and devices containing EEDs be reviewed and tested (if deemed necessary) and positive certification obtained that they can be handled with impunity in the maximum predicted electromagnetic environment before introduction for service use. Three classifications pertinent to HERO for ordnance items have been established. The classifications are based on weapons susceptibility. The degree of susceptibility is dependent upon the electromagnetic environment, the potential for the induction of electromagnetic energy into the ordnance system, and the characteristic of the EED. Items that are negligibly susceptible and require no field intensity restrictions beyond general requirements during all phases of normal employment are classified as HERO SAFE ORDNANCE. Items that are moderately susceptible and require field intensity restrictions for at least some phases of employment are classified as HERO SUSCEPTIBLE ORDNANCE SYSTEMS. Items that are highly susceptible and require severe field intensity restrictions for some or all phases of employment are classified as HERO UNSAFE ORDNANCE.

An extensive testing program exists to define HERO problem areas and ensure the safety and reliability of

ordnance items. Tests are conducted in the maximum RF environment to which ordnance items will be exposed during the stockpile-to-launch sequence. This implies that HERO SAFE ORDNANCE items have been tested to be safe and reliable in the criteria environments.

c. Hazards of Electromagnetic Radiation to Fuels (HERF)

The possibility of accidentally igniting gasoline at shore facilities and aboard aircraft carriers and other ships handling fuel has been considered when rf-induced sparks have been observed. Many years ago the Navy conducted extensive tests and investigations of ignition of fuel vapors by rf-induced sparks and was found that the risk of ignition was small because the following conditions must occur simultaneously for ignition to take place:

(1) Fuels must be heated above their flash points. Fuels will not ignite unless oxygen is provided in certain specific and exact proportions. Fuels will also not detonate unless certain exact proportions of oxygen and fuel are maintained.

(2) Sufficient energy must be provided to sustain ignition. Although radiant energy is the primary source of energy associated with HERF phenomena, no mechanism exists by which this energy can interact directly with the fuel. Radiated energies are capable of causing arcing in susceptive structures. It is these arcs which produce ignition of the fuels.

An arc is a voltage breakdown between two fixed electrodes. It takes a certain amount of voltage to break down the dielectric between the electrodes, but it takes energy behind this source of voltage to sustain the arc for sufficient duration to ignite fuel mixtures. A spark, on the other hand, is formed when two metallic objects in electrical contact are separated and there is sufficient energy between these electrodes to sustain the spark and thus cause the ignition. This is similar to the situation in which a fueling nozzle is withdrawn from the tank opening when an aircraft is being fueled. The radiation field intensity in the proximity of a radiating antenna could be sufficient to induce the required energy.

From actual measurements, it has been determined that a spark of energy of 50 V-A is required to ignite gasoline in an explosive vapor test device. Recently, some attempt has been made to relate the fuel hazard to electric field intensity, the primary result has been to show that the igniting electric field intensity is a function of frequency and is minimal in the upper hf band.

In recent years, the probability of occurrence of this particular hazard has been further decreased with the following advances of technology:

(1) Ship Design. In the design of ship topside arrangements, the location of fuel handling stations, fuel vents, etc, is considered relative to the

placement of RF transmitting antennas. Every effort is made to locate these antennas away from the fuel stations and vents.

(2) Fuel Nozzle Modifications. Heat shrinkable tubing is applied to nozzles used in conventional gasoline fueling. This prevents metal-to-metal contact between the nozzle and the filler tube, thus eliminating the possibility that a spark will occur. Another hazard-reducing development in the aircraft refueling area has been the introduction of the pressurized fueling approach. In this procedure, the fuel nozzle contacts the metallic filler tube of the aircraft prior to the opening of the valve to the tank. Thus, if a spark should occur, there would be no flammable fuel-air mixture to ignite.

(3) Fuel. The type of fuel now being most extensively used is JP-5, which has low volatility compared to gasoline. Because JP-5 does not have the volatility of gasoline, it is not likely to produce flammable fuel-air mixtures under accidental circumstances, this has done much to reduce the fuel hazard aboard ships. The fuel oil which powers the ships is still less flammable than JP-5.[Ref. 4:pp. 4-9]

LIST OF REFERENCES

1. Naval Ocean Systems Center, Technical Document 168, Calculated Electric Near of Navy Shipboard Hf Antennas by J. C. Logan and J. W. Rockway, pp. 1-9, March 1978.

2. Bhattacharya, S., Long, S. A., and Wilton, D. R., "The Input Impedance of a Monopole Antenna Mounted on a Cubical Conducting Box", IEEE Transactions on Antennas and Propagation, Vol.AP-35, No.7, pp. 756-761, July 1987.

3. Lawrence Livermore National Laboratory, Report UCID-20970, Enhancements and Limitations of the Code NEC for Modeling Electrically Small Antennas, by G. J. Burke, January 1987.

4. Lawrence Livermore National Laboratory, Report UCID-21196, Treatment of Small Wire Loops in the Method of Moments Code NEC, by G. J. Burke, October 1987.

5. Yaghjian, A. D., "An overview of Near-Field Antenna Measurements", IEEE Transactions of Antennas and Propagation, Vol.AP-34, No.1, pp. 30-43, January 1986.

6. Naval Ocean Systems Center Technical Document 116, NUMERICAL ELECTROMAGNETIC CODE (NEC) - Method of Moments, by G. J. Burke and A. J. Poggio of Lawrence Livermore Laboratory, January 1981.

BIBLIOGRAPHY

Brown, R. G., Sharpe R. A., Hughes W. L. and Post R. E. Lines, Waves, and Antennas, John Wiley & sons, Inc., 1973.

Cheng, D. K. Field and Wave Electromagnetics, Addison-Wesley, 1985.

Jordan, E. C. and Balmain, K. G. Electromagnetic Waves and Radiating Systems, Prentice-Hall, 1968.

Ramo S., Whinnery J. R. and Van Duzer T. Fields and Waves in Communication Electronics, John Wiley & sons, Inc., 1984.

Stutzman, W. L. and Thiele, G. A. Antenna Theory and Design, John Wiley & Sons, Inc., 1981.

INITIAL DISTRIBUTION LIST

		No. Copies
1.	Defense Technical Information Center Cameron Station Alexandria, VA 22304-6145	2
2.	Library, Code 0142 Naval Postgraduate School Monterey, CA 93943-5002	2
3.	Chairman, Code 62 Department of Electrical Engineering Naval Postgraduate School Monterey, CA 93943-5000	1
4.	Dr. Richard W. Adler, Code 62AB Naval Postgraduate School Monterey, CA 93943-5000	10
5.	Prof. Harry Atwater, Code 62An Naval Postgraduate School Monterey, CA 93943-5000	1
6.	Capitán de Corbeta Carlos R Molina T Comandancia de la Armada Av. Vollmer San Benardino Caracas, 1011 Venezuela	5
7.	Escuela Naval de Venezuela Director Comandancia de la Armada Av. Vollmer San Benardino Caracas, 1011 Venezuela	2
8.	Escuela de Postgrado de la Armada Director Comandancia de la Armada Av. Vollmer San Benardino Caracas, 1011 Venezuela	2

9. Director de Armamento y Electronica — 2
Comandancia de la Armada
Av. Vollmer San Benardino
Caracas, 1011
Venezuela

10. Director de Comunicaciones — 2
Comandancia de la Armada
Av. Vollmer San Benardino
Caracas, 1011
Venezuela

11. Comandante de la Escuadra — 2
Comandancia de la Armada
Av. Vollmer San Benardino
Caracas, 1011
Venezuela

12. Escuela Superior de Guerra Naval — 2
Director
Comandancia de la Armada
Av. Vollmer San Benardino
Caracas, 1011
Venezuela

13. Lt. Eliniadis Panos — 1
461 de la Vina Av. 201
Monterey, CA 93940

14. Lt. Almetlaq — 1
NPGS, SMC 1619
Monterey, CA 93940

15. Donald Wehner — 1
NOSC, Code 744
San Diego, CA 92152

16. Richard D Albus — 1
IIT Research Institute
207 Woodloch LN
Severna Park, MD 21146

17. W.P Averill, Capt. 1
U.S. Naval Academy
Dept. of Elec. Eng.
Annapolis, MD 21402

18. Dr. Duncan C. Baker 1
Elec. & Comp. Eng. Dept.
University of Pretoria
0002 Pretoria, S. Africa

19. John Belrose 1
CRC/DRC, Bldg. 2A, Rm. 330
3701 Carling Av. Box 11490
Sta.H, Ottawa, Ontario, Canada K2H852

20. J.K. Breakall 1
Lawrence Liv. Nat'l Lab.
P.O. Box 5504, L-156
Livermore, CA 94550

21. G Burke 1
Lawrence Liv. Nat'l Lab.
P.O. Box 5504, L-156
Livermore, CA 94550

22. Donn Campbell 1
TRW Mil. Elex. Div.
RC2/266 7X
San Diego, CA 92128

23. Mr. Brent Campbell 1
ECAC, MS 21
North Severn Naval Base
Annapolis, MD 21401

24. Al Christman 1
Ohio University
Stocker Center
Athens, OH 45701

25. Dawson Coblin 1
Lockheed M & S Co.
O/6242;B/130/ Box 3504
Sunnyvale, CA 94088-3504

26. Dave Faust 1
Eyring Research Inst.
1455 W 820 N
Provo, UT 84601

27. D. Fessenden 1
Naval Underwater Sys. Ctr.
New London Laboratory
New London, CT 06320

28. A.W Guy 1
University of Wash.
Biolectromag. Res. Lab.
Seattle, WA 98195

29. G.H. Hagn 1
SRI International
1611 N. Kent Street
Arlington, VA 22209

30. J.B. Hatfield 1
Hatfield & Dawson
4226 Sixth Av., N.W.
Seattle, WA 98107

31. Jackie Ervin Hipp 1
S.W. Res. Inst/ Ema
P.O. drawer 28510
San Antonio, TX 78284

32. Robert Latorre 1
LLNL
L156/Box 5504
Livermore, CA 94550

33. Mr. Jim Logan 1
NOSC Code 822 (T)
271 Catalina Blvd.
San Diego, CA 92152

34. Commander 1
USAISEIC/ASBI-STS (Janet McDoland
FT. Huachuca, AZ 85613-7300

35. E.K. Miller 1
Rockwell Science Center
Box 1085
Thousand Oaks, CA 91365

36. C.A. Nelson 1
NOSC
271 Catalina Blvd.
San Diego, CA 92152

37. I.C. Olson 1
NOSC Code 822 (T)
271 Catalina Blvd.
San Diego, CA 92152

38. David J. Pinion 1
1215 S. Alfred St.
Los Angeles, CA 90035

39. T. Roach 1
Microcube Corp.
Box 488
Leesburg, VA 22075

40. R. Royce 1
Naval Research Lab
Washington, DC 20375

41. T. Simpson 1
University of S. Carolina
College of Engineering
Columbia, SC 29208

42. W.D Stuart 1
IIT Research Institute
185 Admiral Cochrane Dr
Annapolis, MD 21402

43. Richard Tell 1
USEPA ORP
P.O. Box 18416
Las Vegas, NV 89114

44. James Tertocha 1
C-15 Tenbytowne Apts
Delran, NJ 08075

45. Maj. IDF Katzir Joel 2
NPGS SMC 2421
Monterey, CA 93943

46. Lt. Augusto Zapata 1
NPGS SMC 1249
Monterey, CA 93943

47. Director of Research Administration 1
Code 012
Naval Postgraduate School
Monterey, Ca 93943

48. Chief of Naval Operations 1
Code OP-04
Washington DC 20350